Directional Pair-Correlation Analysis of Fracture Networks

François Bonneau, Dietrich Stoyan

Directional Pair-Correlation Analysis of Fracture Networks

François Bonneau [1] **and Dietrich Stoyan** [2]

[1]Université de Lorraine, CNRS, GeoRessources, F- 54000 Nancy, France
[2]Institut für Stochastik, TU Bergakademie Freiberg, 09596 Freiberg, Germany

Key Points:

- Variability statistics of fracture networks are based on distances between object centers measured in dominant directions.
- An artificial network of a simple structure serves as benchmark.
- Important aspects of spatial correlation and variability become visible and measurable by means of pair correlation functions.

Corresponding author: François Bonneau, `francois.bonneau@univ-lorraine.fr`

Abstract

We analyze statistically fractures on surface exposures, which may be considered planar sections through three-dimensional fracture networks (FN). For this planar case, there exist established statistical methods which yield first-order or mean-value characteristics such as fracture density, fracture length distribution or rose of directions.

We extend this situation by presenting a statistical second-order theory, which aims to characterize the inner variability of planar FN. For this purpose we use ideas from the theory of marked point processes or object models, where the 'points' are centers of fractures or fracture branches and the 'marks' are lengths and strike azimuths. The statistics are based on oriented distances between object centers. These distances are represented by so-called pair correlation and mark correlation functions, which we recommend as new variability characteristics for fracture networks. The form of the corresponding plots gives information on the degree of randomness, on most frequent inter-center distances, and on possible local order, all with respect to fracture directions.

We demonstrate the application of these ideas by analysis of three FN. First, we study a synthetic structure, serving as a benchmark to test the methods under ideal conditions. Then, we analyze two field exposures already studied in the geological literature: a well developed and highly connected FN and a highly irregular FN with many small and isolated fractures. The different spatial arrangements of fractures are characterized by the correlation functions.

Plain Language Summary

The existence of rock fractures has a tremendous impact on rock bodies, on their stability, on their hydraulic properties and others. Therefore, describing and understanding the geometry and organization of fracture networks is an issue for both academic and industrial communities.

One way to tackle this problem is to study fracture network geometries at surface exposures, which are irregular and call for statistical analysis. A classical first step of statistics is the determination of the number and density of fractures. The present paper aims to contribute to the next step, by presenting methods for the description of the variability of fracture networks. Its basic idea is to describe each fracture by a point, its center, which holds two marks, length and orientation of the fracture, and then to use methods for statistical analysis of point patterns. In particular, the distances between the fracture centers are analyzed statistically, measured in the dominant directions of the network. The results are presented in various plots of correlation functions, yielding information on degree of randomness and local order.

The application of this method is demonstrated for a synthetic and two natural fracture networks. The natural network show clear differences in the spatial distribution of fractures, which are well presented by the plots. The synthetic network serves as a benchmark.

1 Introduction

Fractures are mechanical discontinuities in rocks, visible on surface exposures as fracture traces. They form complicated spatial networks called fracture networks (FN), which have a complex geometry and spatial organization. Such networks have great influence on the stability of rock bodies, on ore deposits, on fluid flow and, on reservoir capacity and compartmentalization. Therefore FN are a topic of intensive research, see e.g., Hardebol et al. (2015); Lei et al. (2017); Peacock and Sanderson (2018); Laubach et al. (2019); Sui et al. (2019), and references therein for recent reviews and case studies).

A complete and objective description of FN as three-dimensional objects is extremely difficult as they cannot be observed directly. Methods such as core or log analysis provide only small-scale and sparse observations. Geophysical surveys provide complementary data at larger scale and miss the detection of small fractures, i.e. smaller than the wavelength of the signal propagated. In the end, well data need to be interpreted and extrapolated using physical and mathematical methods to build a consistent description of a natural FN.

As in many other publications, we study the fracture traces on surface exposures, which we will further refer to as 'fractures'. By their nature, they are cross-sections of the corresponding three-dimensional FN. Such sections provide valuable information in the context of modeling of three-dimensional FN, see e.g., Bonneau et al. (2016). When testing the quality of simulated or synthetic FN, planar sections may be compared with exposure patterns paving the way to realistic three-dimensional FN modeling. For this purpose, it is important to characterize a planar FN with informative parameters and statistical summary functions.

Following the example of Bonnet et al. (2001); Darcel et al. (2003b, 2003a), we consider FN as samples of 'object models' (Pyrcz & Deutsch, 2014), i.e. of marked point processes where the 'marks' are geometrical objects, in our case straight-line segments that represent fractures or pieces of fractures called branches. The 'points' are the centers of these objects, which are characterized in a natural way by trace length and orientation marks.

For these FN, there exist an established first-order[1] theory, which is presented in Zeeb et al. (2013). 'First order' means that spatial mean-values are determined such as fracture density, average number of fractures per area unit. While these characteristics are valuable for a general or global description, they tell nothing about the spatial variability of FN nor about their inner spatial correlations, and so are not sufficient for rigorous model testing. This was already mentioned by Dershowitz and Einstein (1988), who briefly discussed some early papers in the context of 'autocorrelation and correlation' of FN.

For the definition of second-order[2] characteristics for FN, this paper uses ideas of spatial and point process statistics. The marked-point-process approach offers well-established functional summary characteristics, which we recommend as descriptors of variability behavior. Most of them have names that contain the word 'correlation' and they are indeed related to the well-known correlation functions of geostatistics. In most modern papers related to statistics of marked point processes, isotropy is assumed. Here, we consider anisotropy as an essential feature and use modified direction-dependent correlation functions. Even, we perform a separate analysis of subfamilies of objects with similar orientation.

The methods we describe are applicable to fractures as well as to fracture branches. The analysis of fracture center systems yields information about the spatial distribution of fractures, while the analysis of branch centers helps to characterize aspects of the interaction of fractures.

We apply our methods to the analysis of data from one synthetic and two natural FN, for comparison. The first natural FN is given by a map from a satellite image of the Oman mountains and the second is a surface exposure from the Hornelen Basin in Norway. These data were already studied respectively in Zeeb et al. (2013) and Odling

[1] The statistical term 'first-order' should not be confused with 'primary' as used in the term 'primary FN characteristics' in Dershowitz and Einstein (1988).

[2] The statistical term 'second-order' should not be confused with 'secondary' as used in the term 'secondary FN characteristics' in Dershowitz and Einstein (1988).

(1997) by means of first-order methods and by fractal methods (Darcel et al., 2003a, 2003b). Second-order statistics add variability aspects to the description of these patterns.

2 Fundamentals of FN Characterization

The geometrical-statistical investigation of FN is a well-known challenge. Therefore, here the usual geological approach combining field observations and modeling is applied. This section presents a brief overview of useful mathematical models, simplifications and statistical estimators.

2.1 Modeling FN

A really accurate way to describe an FN would explicitly represent fractures as individual objects in the spirit of object models (Pyrcz & Deutsch, 2014). Each fracture is then characterized by its spatial location, i.e. a point x_n, and its own irregular geometry, given by a set X_n.

Statistics for all the X_n are a rather difficult task, even if the fractures were fully observable. Therefore and since the observation conditions are usually limited, FN characterization uses models with various simplifying assumptions. The most common mathematical idealization of spatial FN is to consider them as systems of two-dimensional flat surface pieces, i.e., the X_n are assumed to be planar objects such as discs, ellipses or rectangles. This means that apertures and deviations from flat shape are ignored.

These X_n are randomly scattered in space, where 'randomly' does not mean 'without any rules' or 'totally irregular'. In fact, in natural FN there are various spatial correlations between the fractures: younger fractures may be stopped by older ones, in the close neighborhood of fractures there is often space without fractures resulting from stress reduction in the shadow zone.

A classical model for three-dimensional FN is the Poisson-Baecher disc model, an object model, where the location points x_n are a homogeneous Poisson process[3] and the objects X_n are discs (Dershowitz & Einstein, 1988). The planar counter-part of a Poisson-Baecher disc model is a so-called Poisson-Boolean segment process (Chiu et al., 2013), where the planar points x_n form a planar homogeneous Poisson process[4] and the objects X_n are linear segments. Some modern object models for FN are discussed in Stoyan (2021), focusing on the papers Koike et al. (2015); Ivanova et al. (2014); Cherpeau et al. (2010); Cherpeau and Caumon (2015); Bonneau et al. (2016).

In the present paper, planar FN are considered, which can be understood as resulting from planar sections through three-dimensional FN. In this planar setting, FN means 'planar FN', and the fracture traces are approximated by straight-line segments X_n (in the following: segments). The corresponding location points x_n are the segment centers in the considered plane. This is a pure geometrical choice, since the segment centers are hardly related to points where the segments start to grow. The segments are characterized by two real marks: their length l_n and azimuth angle a_n. The a_n are angles ($\in [0^c irc, 180^\circ[$) between the north and segment direction, measured in clockwise order. Thus, each fracture is uniquely described by a marked point $[x_n; (l_n, a_n)]$. In this way an FN is modeled by a random collection of marked points.

Such collections are called in mathematics marked point processes. These are random sequences of location points x_n associated with marks, which are in this case vec-

[3] In an homogeneous Poisson process, points are uniformly distributed in space.

[4] Indeed, it can be shown that the planar section through a Poisson-Baecher disc model yields a collection of segments, which centers form a planar homogeneous Poisson process (Chiu et al., 2013).

tors (l_n, a_n). The theory and statistics for marked point processes are described in books such as Illian et al. (2008) and Baddeley et al. (2016). There are many distributional characteristics of marked point processes, which are explained in this paper when needed.

We mention here that there is an alternative approach to statistical modeling and analysis of FN. Instead of individualize an FN as a set of objects, the whole FN can be taken as a sample of a segment system. In this way, there is no need to define objects, but some information about the geometry, about the inner organization and perhaps also about the genesis of an FN may be lost.

This mathematical idea goes under the title 'segment process' as in Chiu et al. (2013), chapter 8, and Stoyan (2021). Some characteristics classically used by geologists can be seen as belonging to this theory. These are the rose of directions (when including the length of traces) and the total length of fracture traces per area unit. Also studies of intersections of FN with scan-lines and statistical investigations of sequences of intersection points can be considered following segment-process reasoning.

2.2 Fractures and Fracture Branches

This paper describes FN by patterns of segments that stand for fractures or for parts of a fracture called 'branches'.

For the construction of segments that represent fractures, we connect their two endpoints by straight lines and ignore deviations from a linear form (Figure 1 (a) and (b)). This representation is not always unique since it is not always clear where a fracture ends (Figure 1 (b1) and (b2)).

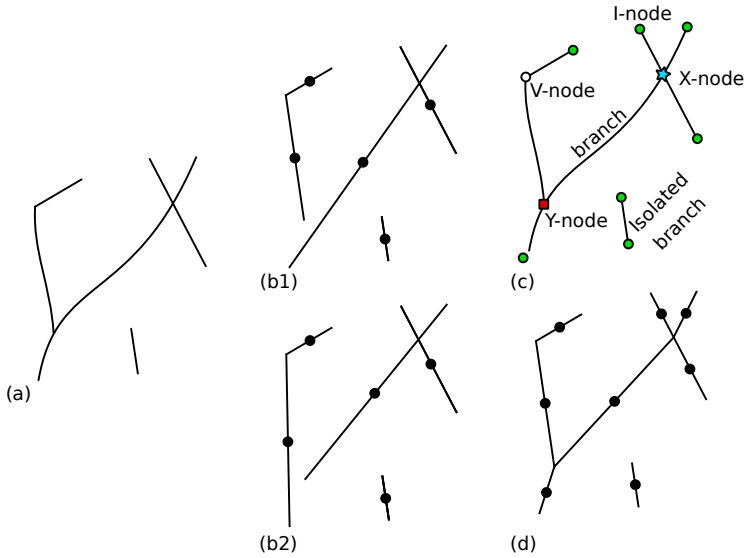

Figure 1. A small piece of a planar FN described as a marked point pattern. (a) A planar FN, (b1) and (b2) two possible representations of the FN in (a) with segments standing for fractures, while the points are fracture centers, (c) topological scheme with branches and nodes, (d) unique representation of the FN in (a) with segments standing for fracture branches; now the points are branch centers.

The definition of branches uses the topological scheme introduced by Sanderson and Nixon (2015); Saevik and Nixon (2017). The original FN is equipped with nodes of four types that characterize the topology of the FN. The four types are, see Figure 1 (c):

- I-node: isolated end-point of a fracture,
- V-node: connects two fractures at their tips,
- Y-node: connects two fractures, one stops on the another (not at its tip),
- X-node: crossing point of two fractures.

The original fracture branches are curves between nodes. For the statistical analysis these branches are replaced by straight-line segments that connect the two end-points of the original branches (Figure 1 (d)). In the following, we simply call these segments 'branches'.

The approximating segment differs from the geometry of the original fracture and branch; the deviation is usually smaller for branch than for fracture.

Each segment is considered as an object in the sense of object models. Its center is the corresponding point x_n, and its geometrical information is condensed in two real numbers (l_n, a_n), length and azimuth, as defined in Section 2.1. This leads to the classical case of marked point processes with real-valued marks, and the standard methods from point process statistics can be applied.

In practical work, the determination of the points x_n for fractures and branches is a non-trivial problem because of edge-effects. Our solution is explained here for fractures: If a fracture is fully in the window, the x_n is simply the center of the corresponding segment. If a fracture is not fully in the window, there are two options according to the size of the segment inside. Either it is shorter than the median of fracture length distribution, then no point is constructed, or it is longer and x_n is the center of the segment-part in the window. Note that not constructing a point for a segment does not mean that it is excluded from the statistics. The segment is considered in the first-order characterization, but excluded from the second-order characterization.

The question of which objects one should use remains: fractures or branches? The decision matters because the second-order statistics are carried out for the object centers and their marks—and the patterns of the corresponding centers differ greatly, in number and distribution. It is obvious that fractures are often very long and their centers are therefore in large distances from big parts of the objects they represent. In contrast, the branches are shorter and their centers are closer to the ends. The following shows that both approaches have their benefits, depending on the nature of the FN considered.

2.3 Homogeneity

In statistical analyses of spatial data the statistician often targets global conclusions for the whole window of observation. In the FN context this may hold for the global density of fractures. Similarly, the methods discussed in this paper can be used to obtain statements about global variability of FN. Of course, this only makes sense if everywhere in the window there are the same chances to observe similar fluctuations.

The mathematical formulation of this property goes under the name 'homogeneity'. Because of the wide application of this idea, there are equivalent names for the property, namely 'statistical homogeneity' and 'stationarity'. The latter is used in the context of point processes. Here, we use the term 'homogeneity'.

A geometrical structure is called *homogeneous* if the statistical distributions of its elements are invariant with respect to spatial translations (Chiu et al., 2013) For a marked point process, in particular, this implies that (1) the local point density fluctuates everywhere around the same value and (2) the marks show everywhere similar variability. Then, it makes sense to speak about a global value of point density, and a global distribution of mark values.

It is clear that homogeneity is a mathematical concept, which may be true for theoretical stochastic models of FN. When a real FN is investigated, it is a fundamental decision of the geologist together with the statistician to decide if the FN can be considered as a homogeneous structure. This assumption is not justified if there are, for example, clear spatial trends in fracture density or erratic deformations of the FN. The paper Sanderson and Peacock (2019) with its studies of fracture swarms and corridors is a good example of statistics in the case of inhomogeneity.

Sometimes, an FN can be partly affected by a local deformation. In that case, the homogeneity hypothesis may call for a restoration to remove translation and/or rotation due to such a deformation (Bergbauer & Pollard, 2004; Macé et al., 2004). Geologists may keep that in mind and use their knowledge to isolate sub-regions where the homogeneity assumption is acceptable. Bistacchi et al. (2020) give an excellent example of such a regionalization. On the other hand, the size of the window has some influence, a small part of a large homogeneous structure may look like an inhomogeneous pattern.

There exist another geometrical invariance property called *isotropy*, which means invariance of distributions with respect to rotations. For FN, this property appears to be totally unrealistic, perhaps with the exception of micro-structures. However, we use statistical summary characteristics that belong to the isotropic case and consider them as directional averages.

2.4 Fracture Density Measures

Fracture statistics uses a classical system of numerical measures to quantify the amount of fracturing in rock masses (Dershowitz & Herda, 1992; Dershowitz et al., 2020). It is (implicitly) based on the assumption of homogeneity, and therefore care is necessary in its application. The characteristics are given in a notation system which contains symbols of the form P_{ij}, where 'P' means 'persistence' (Dershowitz & Einstein, 1988), i denotes the dimension of the measurement region and j the fracture attribute. Here, we only discuss the planar characteristics, namely *fracture density* P_{20} and *fracture intensity* P_{21}.

The first denotes the mean number of fractures per area unit. In object process thinking, where each fracture is represented by a marked point, this is a fundamental point-process characteristic. This characteristic is called 'intensity' in the point process theory, and corresponds to the mean number of points per area unit. Here, we use geological terms and notation to discuss the number of objects per area unit. Different values of P_{20} appear when for the same pattern fractures and branches are considered in parallel. For the statistical estimation of P_{20}, it is recommended to count the number of lower end-points of segments, and then to divide it by the window area, see e.g. Chiu et al. (2013) p. 250, Zeeb et al. (2013), and Sanderson et al. (2019).

The second characteristic, fracture intensity P_{21}, is the mean of total fracture trace length per unit area. Various techniques exit for its statistical determination, see Chiu et al. (2013); Zeeb et al. (2013). Starting with a map of the surface exposure, methods of image analysis enable direct determination of the total length of all fractures even if they are curved. If the data are given as sets of linear segments, it is even simpler. The values of P_{21} for fractures and branches may differ a little.

2.5 Lengths and Orientations

The lengths l_n of fractures or branches are important quantities of FN. Their values are characterized by a distribution function, the *fracture (or branch) length distribution function*. In the theory of marked point processes, such a distribution is called a mark distribution.

The best and simplest method to estimate the mean length of fractures (or branches) is to use the total length of all segments in the window and divide it by the total number of lower end-points. In this way, edge-effects are eliminated. In contrast, the precise estimation of length distributions is a difficult task, because of edge-effects, which play an important role for small windows. We recommend and use in this paper the Miles-Lantuejoul estimator with minus-sampling, which is explained in Appendix A.

Various types of theoretical distributions have been used for the lengths, perhaps the power-law is still the most common choice, but log-normal, exponential and gamma distributions are also used, see Bonnet et al. (2001).

Since segments are fully characterized by position, length and orientation, orientations are also indispensable characteristics in the study of FN. Statistically it makes little sense to study a directional mark distribution of the a_n. This way, short and long fractures or branches would count equally. Therefore FN statistics collects the directional data in the well-known *rose of directions* or *rose diagram*, which is simply a length-weighted distribution of directions.

The orientations of fractures are closely related to the genesis of FN. Natural FN are composed of collections often called 'fracture sets', which contain fractures with similar orientation, determined by the global stress responsible for the fracturing event. These fracture sets play a central role in this paper.

2.6 Fracture Spacing and Scan-Lines

A classical method to study the spatial organization of FN is analysis of fracture spacing (distances between fractures) along scan-lines. These lines are often oriented perpendicularly to the main fracture strike azimuth. The intersection points with fractures on the lines are statistically analyzed using methods for point processes on the real line.

This means to study the distances between successive points, and to consider the corresponding distribution functions and probability densities, assuming homogeneity (Bistacchi et al., 2020). Deviations from the homogeneous one-dimensional Poisson process, the model of complete randomness of point distribution, are of special interest. In that case, the distance distribution is an exponential distribution and the distances are independent. As a measure of comparison the coefficient of variation Cv[5] is used (Gillespie et al., 1993, 1999). Indeed, $Cv = 1$ indicates exponential distribution, while $Cv < 1$ indicates a tendency to regularity, and $Cv > 1$ an irregular distribution such as clustering.

The paper Shakiba et al. (2022) introduced second-order statistics for fracture spacings: the one-dimensional analogue of Ripley's K-function (Section 3.1). This way clustering and regularity can be described better than by simple comparison with the Poisson process.

The paper Sanderson and Peacock (2019) is an example of analysis under inhomogeneous conditions. There the spacings are analyzed in order to characterize swarms and corridors of fractures.

2.7 Connectivity

The connectivity of an FN is an important aspect of their characterization because of its impact on the physical behavior of fractured rock. A complete review of all connectivity measurement is out of the scope of this paper. The interested reader may refer to Manzocchi (2002); Renard and Allard (2013); Sanderson and Nixon (2018) and

[5] Cv is the standard deviation of the distribution of spacing divided by its mean.

the references therein for an overview of interesting connectivity metrics. The number of intersections per fracture (C_f) has been largely used particularly in the context of percolation theory (Balberg & Binenbaum, 1983; Berkowitz, 1995; Manzocchi, 2002).

More generally, most of connectivity metrics can be defined in the frame of graph theory. The idea behind is to quantify and characterize intersections of fractures. The topological scheme presented in Section 2.2 is in the spirit of graph theory, where the nodes of the graph are fracture intersections and end-points (I, V, Y and X nodes) and where fracture branches are graph edges. This representation has been used to classify FN using the relative proportion of I,Y and X nodes (Manzocchi, 2002; Sanderson & Nixon, 2018; Sanderson et al., 2019).

In the present paper, we use both the average number of intersections per fracture C_f and the proportions of I,Y and X nodes.

3 Second-Order Characteristics for FN

Second-order characteristics describe the variability of random structures; *variance* and *correlation* are standard terms in this context. Indeed, the variability of a point pattern could be described by the variance of point number in a test circle randomly placed in the pattern. However, the variance obtained would depend on the circle radius; and when using, for example, test squares, other values of variances would be obtained. Therefore, the statistical theory of point processes uses another approach and employs various correlation functions. These functions can be used to calculate, by integration, the variances of random variables (e.g., the number of points or sum of marks) in a test area defined by its size and shape (Chiu et al., 2013; Illian et al., 2008).

The main application of these functions in spatial statistics is the direct characterization of certain aspects of spatial variability. The corresponding statistical estimators work in the center-to-center manner, using point pairs, their inter-point distances and their marks. These distances are then statistically analyzed.

In the present paper, marked point processes are always considered to be homogeneous but anisotropic. Nevertheless, in the explanation of the statistical estimators, isotropy is assumed for better understanding. Also, the corresponding isotropic characteristics play some role as directional averages.

In the following part, we explain various second-order characteristics for marked point processes. We start with characteristics that describe only the points, ignoring the marks first. These are Ripley's K-function $K(r)$ and the pair correlation function $g(r)$. The marks are integrated in mark-correlation functions and in anisotropic pair correlation functions $g(r, \theta)$. The latter, which employ essentially segment orientations, are the most important tools in the paper.

3.1 Ripley's K-Function

The explanation of Ripley's K-function $K(r)$ is as follows: Consider a circle of radius r centered at a randomly chosen point of the point process and count the number of points within the circle, not counting the circle center. This number is random, its mean is denoted by $P_{20}K(r)$ and depends on the radius r. Given fracture density P_{20}, this defines $K(r)$.

Clearly, $K(r)$ is an increasing function of r. Its form gives valuable information on the nature of the point distribution. However, since its definition is based on circles, it is a characteristic of an isotropic nature.

For many point process models the form of $K(r)$ is theoretically known. Here, we mention only the simplest case, the homogeneous Poisson point process, the model of complete spatial randomness. For this model with its strong independence properties it holds simply

$$K(r) = \pi r^2 \text{ for all } r \geq 0. \tag{1}$$

For cluster processes Ripley's $K(r)$ has values larger than πr^2, while for regular processes the values are smaller.

The statistical estimation of $K(r)$ follows its definition. Here, we describe a naive estimator without edge-correction (thus with some bias) for $K(r)$. Assuming that there are n points x_i in a window W of area $A(W)$, it is plausible to estimate $P_{20}K(r)$ by

$$\mathbf{K}(r) = \frac{1}{n}\sum_{i=1}^{n} N_i(r), \tag{2}$$

where $N_i(r)$ is the number of points in the circle of radius r centered at x_i (not counting the circle center x_i). An estimator of $K(r)$ is then obtained dividing by an estimator of P_{20}, namely $n/A(W)$. Better estimators of $K(r)$ are described in the literature on point process statistics (Illian et al., 2008; Baddeley et al., 2016).

Clearly, the sum in $\mathbf{K}(r)$ is the same as $n_p(r)$, the number of point pairs in W whose inter-point distances are smaller than r, which is used in fractal statistics (Hentschel & Procaccia, 1983). Then

$$\mathbf{K}(r) = n_p(r)/n. \tag{3}$$

Thus $K(r)$ is closely related to the 'two-point pair correlation function' $C_2(r)$ (Bonnet et al., 2001) defined by

$$C_2(r) = \frac{2n_p(r)}{n(n-1)}. \tag{4}$$

This $C_2(r)$ is used to determine a fractal dimension for fractal point systems: If it scales with r as r^D then the exponent D is called 'correlation dimension'. For dimension estimation, Agterberg (2014) recommends to use edge-corrected estimators of point process statistics, or the pair correlation function (see the discussion below).

3.2 Pair Correlation Functions

Pair correlation functions ('pcf') are the main statistical tools we apply in the present paper. We start with an explanation of the isotropic pcf, which ignores marks and assumes isotropy of the point pattern.

The isotropic pcf $g(r)$ can be formally defined as the derivative of the K-function:

$$g(r) = \frac{K'(r)}{2\pi r}. \tag{5}$$

Thus between $K(r)$ and $g(r)$ there is a relation similar to that between a cumulative distribution function $F(x)$ and the corresponding probability density function $f(x)$.

A heuristic explanation of $g(r)$, which may help in interpretation, is as follows. Consider two deterministic points x and y at distance r. These points are the centers of the infinitesimally small circles $b(x)$ of area $\mathrm{d}x$ and $b(y)$ of area $\mathrm{d}y$. The probability to have a point in $b(x)$ is $P_{20}\cdot\mathrm{d}x$ and for $b(y)$ it is $P_{20}\cdot\mathrm{d}y$. Consider now the probability that there is a point both in $b(x)$ and $b(y)$. Under isotropy assumption this probability depends only on the distance r between x and y. Denote this probability by $p(r)$ and write it as:

$$p(r) = g(r)\cdot P_{20}\mathrm{d}x \cdot P_{20}\mathrm{d}y \tag{6}$$

The factor $g(r)$, which contains the dependency on r, is the isotropic pcf.

In the case of a homogeneous Poisson process, the multiplication theorem of probability theory yields $p(r) = P_{20}\mathrm{d}x \cdot P_{20}\mathrm{d}y$ and $g(r) \equiv 1$ because of the independence property of the process.

For all reasonable isotropic point processes the function $g(r)$ takes for large r the value 1. In fact, for large r, the events 'there is a point in $b(x)$' and 'there is a point in $b(y)$' become independent. Maxima and minima of $g(r)$ mark characteristic values of r, related to typical inter-point distances. Values larger than 1 for small r indicate clustering, while values smaller than 1 appear in the case of regularity.

A pcf can have very large values for small r in the case of strong clustering. The case of $g(0) = \infty$ is even possible for some point process models. In this case one speaks of a pole at $r = 0$. If it is known that the point pattern can be considered as fractal, and if $g(r)$ scales for small r with r^{-H}, then its fractal dimension D is $D = 2-H$. However, non-fractal point processes may also have a pcf with a pole at $r = 0$. Therefore, the existence of a pcf pole is not a proof of fractality (Stoyan, 1994).

For the estimation of $g(r)$ there exists established software (Baddeley et al., 2016), whose fundamentals are explained in Illian et al. (2008). The main idea is counting the number of pairs of points in a given inter-point distance r.

The interpretation of empirical pcfs is not simple, but we will provide the required guidance and interested readers may refer to Illian et al. (2008) for a thorough explanation.

In the form presented here $g(r)$ is a characteristic for the isotropic case. When we use it for anisotropic patterns, we speak about the 'isotropic pcf'. It is understood as an average over all directions and serves as a characteristic giving global inter-point distance information.

However, when we want to include orientations, we work with an anisotropic version of the pcf. The *anisotropic pair correlation function* $g(r, \theta)$ was introduced in Stoyan and Stoyan (1994), p. 286, and is explained in Appendix B. It is statistically estimated by counting the number of pairs of points of a given inter-point distance r and connected by a line of azimuth approximately equal to θ. We use a private implementation for its estimation, which is a simple modification of the standard algorithm for $g(r)$.

3.3 Mark Correlation Functions and Variograms

The mark correlation function $k_{mm}(r)$ characterizes aspects of spatial correlation for a real-valued mark. (The reader may associate the term 'mark' with 'segment length'.) The variable 'r' is as above the distance between points. Here, we explain $k_{mm}(r)$ as we did for $g(r)$ for the isotropic case.

The term $k_{mm}(r)$ is the mean of the product of the marks held by two randomly chosen points separated by a distance r. The estimator considers every pair of points approximately separated by a distance r, and multiplies their marks. The mean of these products is divided by a pair correlation estimator, and by the square of the mean mark $m(l)$. Therefore, $k_{mm}(r)$ has the nature of a conditional mean. A more precise definition can be found in Illian et al. (2008).

If the marks are independent, $k_{mm}(r)$ has the theoretical value of 1 for all r. For small r, $k_{mm}(r)$ values smaller than 1 indicate that close segments tend to have shorter lengths than the mean length of segments in the FN. For large r, as mark values become independent, $k_{mm}(r)$ tends to the theoretical value of 1.

Statistical experience shows that it can be accepted to use mark correlation functions in the analysis of anisotropic patterns. In fact, they are obtained by ratio-estimators, where unwanted fluctuations of numerator and denominator are canceled out.

The *mark variogram* $\gamma_m(r)$ is a function similar nature to $k_{mm}(r)$. Instead of the product of marks the half squared difference is used, and the function is not normalized. The mark variogram can also be used in anisotropic cases, since the absolute values of marks do not play a role but only mark differences.

For large r, the theoretical value of a mark variogram is equal to the variance σ_m^2 of the marks. Values of $\gamma_m(r)$ smaller than σ_m^2 for small r show that the marks of close points tend to be similar.

The statistics of mark correlation functions are described in Illian et al. (2008).

4 Analysis of an Artificial FN

In this section, we study the Poisson-Boolean segment process (Section 2.1) as a very simple stochastic model of an FN, where the segments stand for fractures. This is an analysis under ideal conditions, in order to serve as a benchmark and to help understanding the first- and second-order characteristics of an FN with a high degree of randomness.

We consider a special Poisson-Boolean segment process, with intensity $P_{20} = 0.2$, where all segments have the constant length of 5 m and randomly the three directions 0°, 90° and 130° with equal frequency.

The fracture centers were simulated in a 105×105 square meter window, as uniform random points of density $P_{20} = 0.2$ points per square meter. While the window W in which we operate is 100×100, we started with the larger window in order to avoid edge-effects. So also segments with center outside of W can contribute.

The segments for branches are built from the same realization considering the intersections of fractures.

Figure 2 shows a typical simulation of the model. The fractures are highly connected and produce many branches. We counted only 9.0% isolated fractures. The three subsets of fractures or branches with similar orientations are called N0, N90 and N130.

4.1 First-Order Characteristics

We apply the methods described in Section 2 for the statistical analysis of the simulated pattern.

While the fracture density P_{20} is close to the theoretical value 0.20 (with a small statistical deviation), it is much larger for the branches, namely 0.75 points per square meter.

Concerning the marks, because the fractures are exact linear segments, the roses of directions of fractures and branches are identical, and follow the three chosen directions. In contrast, the distributions of lengths for fractures and branches differ (Figure 3). While the fractures have the constant length of 5 m, the lengths of branches are variable and show a strongly asymmetric distribution, with a median (1.01 m) significantly smaller than the mean (1.36 m). Following the recommendations discussed in Section 2.5 and Appendix A, objects not completely in the observation window are not used to estimate the length distribution. But they are used for estimating P_{21}.

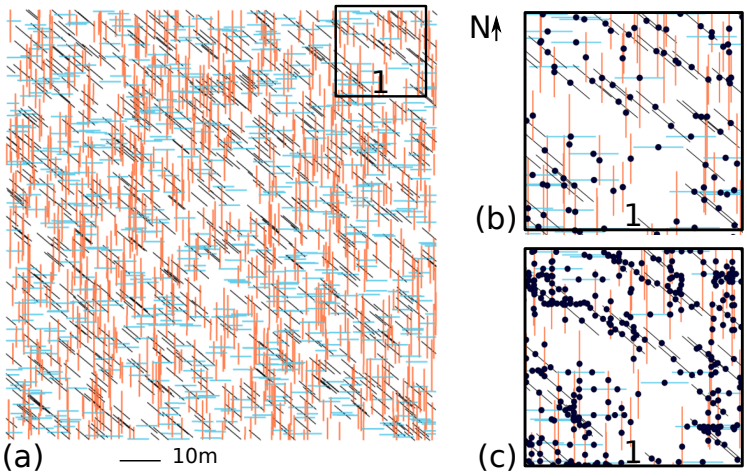

Figure 2. (a) 2D map of the Artificial FN simulated with three fracture sets oriented $0^\circ \pm 5^\circ$ (red), $90^\circ \pm 5^\circ$ (blue) and $130^\circ \pm 5^\circ$ (black). The black square (1) localizes the area shown in (b) and (c). (b) Fracture centers: points of a homogeneous Poisson process. (c) Branch centers constructed by the median rule: a clustered point pattern.

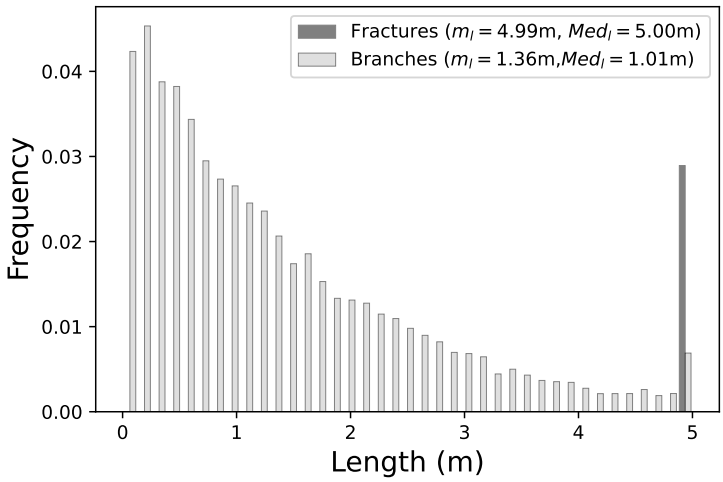

Figure 3. Length distributions of fractures and branches for the Artificial FN (Figure 2).

Table 1. First-order characteristics of the Artificial FN

	Fractures				Fracture Branches			
	Full set	N0	N90	N130	Full set	N0	N90	N130
P_{20} (nb.m^{-2})	0.205	0.0689	0.0677	0.0680	0.750	0.268	0.253	0.230
P_{21} (m^{-1})	1.02	0.340	0.340	0.340	1.02	0.340	0.340	0.340
m_l mean length (m_l) (m)	4.99	4.94	5.02	5.01	1.36	1.27	1.35	1.48
Med_l median length (m)	5.0	5.0	5.0	5.0	1.01	0.96	0.98	1.12
Connectivity								
C_f (nb.fracture^{-1})	2.52	2.76	2.61	2.21				
$p_{I-nodes}$	0.44	0.41	0.44	0.48				
$p_{Y-nodes}$	0	0	0	0				
$p_{X-nodes}$	0.56	0.58	0.57	0.52				

The empirical first-order characteristics for fractures and branches of the three sets N0, N90 and N130 are presented in Table 1. Consistently with findings in Manzocchi (2002), the probability of occurrence of Y nodes in such a stochastic model is very low: Indeed, no Y nodes are in the simulated Artificial FN.

4.2 Second-Order Characteristics

This part focuses on the spatial organization of fracture and branch centers. For these centers, here is a special situation, which is never given with natural data: The exact fracture centers are known. For validation, we carried out the second-order analysis with both the estimated (Section 2.2) and the true fracture centers. We observed no significant differences in the results and report here those from estimated fracture centers. (Note that the median-rule removes all fractures that are not completely inside the window because their length is smaller than the median, which is 5 m.).

Pair Correlation Functions: whole pattern

Figure 4 shows empirical isotropic and anisotropic pcfs for the whole pattern of fractures and branches of the Artificial FN. The directions θ considered for the anisotropic pcf $g(r, \theta)$ are those of fracture strike azimuth of the sets N0, N90 and N130.

The curves for fracture centers (Figures 4 (a)) have a very simple form since they belong to homogeneous Poisson processes: Constant values with small statistical fluctuations around the theoretical value of 1.

In contrast, the pcfs for branch centers have a quite different form. They have very large values for small r and tend to 1 for large r. This is the typical form for so-called cluster processes. It even seems to make sense to assume that there are poles of the pcfs at $r = 0$. This behavior can be explained by the spatial arrangement of branches. Branches are the result of fracture intersections, their centers are aligned on fractures, and their lengths are random. Consequently, many branch centers form sub-patterns similar to pieces of linear Poisson processes. Just a model of similar nature is one presented in Stoyan (1994), where the points are randomly scattered on randomly scattered segments. In that model, the pole of the pcf at $r = 0$ is proved mathematically; it does not result from dense clusters but from the linear arrangement of points.

The pcf values close to 1 for $r > 5$ m are a consequence of the constant fracture lengths: Indeed, for distances larger than 5 m point pairs belong to different fractures and there are no more spatial correlations.

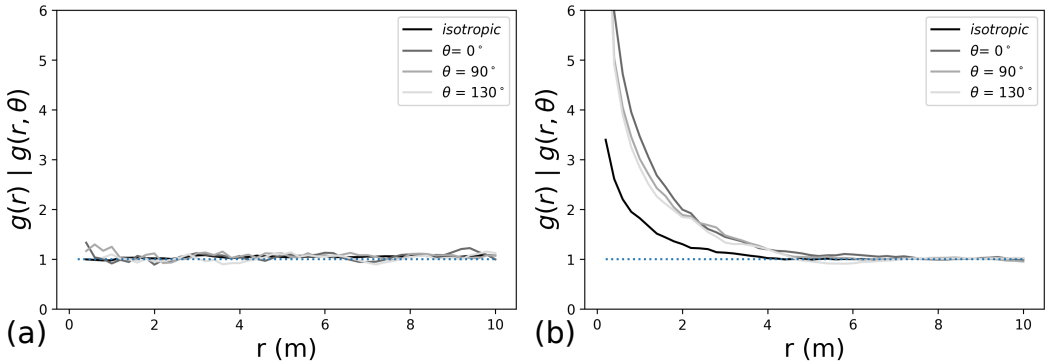

Figure 4. Empirical isotropic pcf $g(r)$ (black curve) and anisotropic pcfs $g(r, \theta)$(gray curves) for the full set of (a) fractures and (b) branches of the Artificial FN. The blue dot curves indicate the theoretical value of 1.

Pair Correlation Functions: Set N0

Now, we focus on the objects of the set N0, which contains all objects with strike azimuth 0° shown in red in Figure 2. The empirical isotropic and anisotropic pcfs are shown in Figure 5. We chose the direction θ corresponding to the azimuth of objects (0°) and the perpendicular (90°).

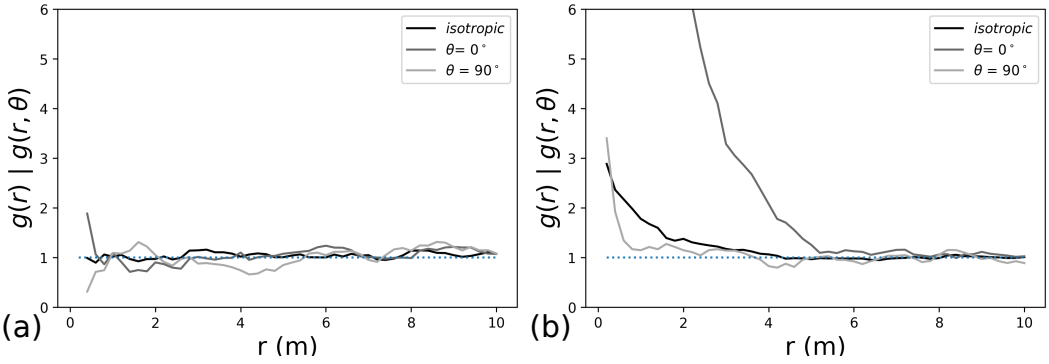

Figure 5. Empirical isotropic and anisotropic pcfs with $\theta = 0°$ and 90° for subset N0 for fractures (a) and branches (b) of the Artificial FN.

We observe a similar behavior to the one of the full set, and for the other subsets N90 and N130 it is similar as well. For fractures, the centers of the N0 subset belong again to a homogeneous Poisson process and this also holds for the other subsets (N90 and N130). For branches, the explanation of the large values of $g(r, 0)$ for small r is similar to the one for the full set. They result from sequences of points aligned on fractures. In the direction 90°, orthogonal to fractures, points are not aligned and $g(r, 90)$ has smaller values than $g(r, 0)$ for small r.

Mark Correlation Functions and Variograms

The empirical mark correlation functions $k_{mm}(r)$ and mark variograms $\gamma_m(r)$ for the lengths of fractures and branches of the Artificial FN are shown in 6.

For the fractures $k_{mm}(r)$ reflects the simple situation of constant marks: It is constant and equal to 1. In this case, the mark variograms also follow the theory with a constant value equal to 0. Indeed, because the fracture lengths are constant, their differences vanish and the corresponding variance is zero.

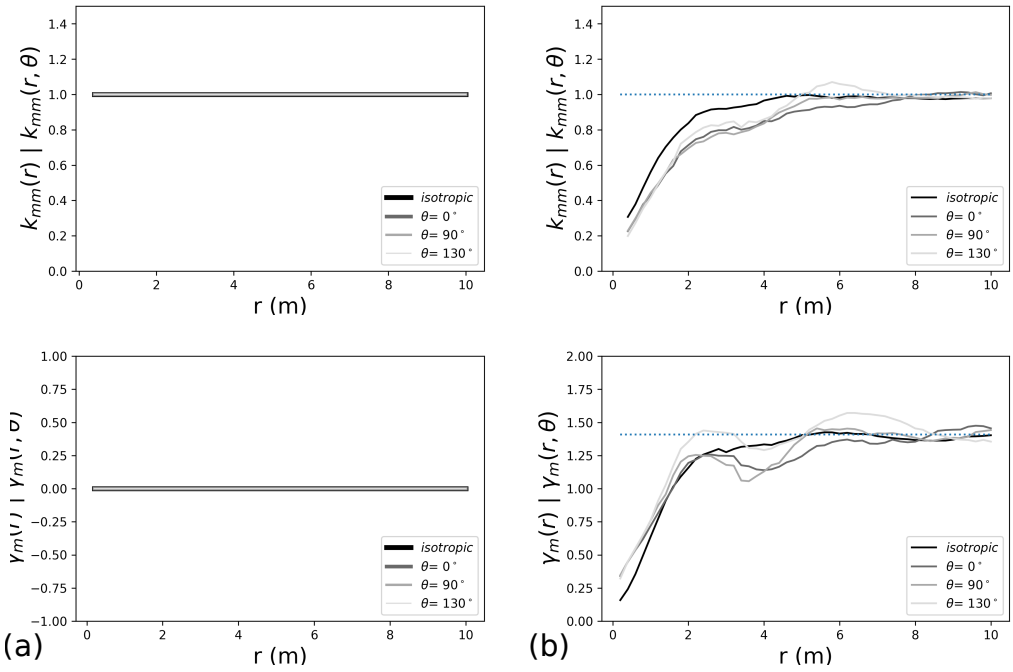

Figure 6. Empirical 0°, 90°,130° anisotropic and isotropic mark correlation function ($k_{mm}(r)$) and mark variogram ($\gamma_m(r)$) for fractures (a) and branches (b) of the Artificial FN. The theoretical values expected for large r are shown as the dotted blue lines.

In contrast, for the branches there is non-trivial spatial length-mark correlations, as shown by Figure 6 (b). The original constant fractures are randomly divided, which results in random branch lengths, see Figure 3. The form of $k_{mm}(r)$ shows that close branches tend to have smaller lengths than the average. Indeed, by the construction of branches frequently short branches are close together, resulting from intersections of the same fracture. Note that the form of the length distribution function shows that almost 62% of branches are shorter than the mean.

The range of correlation is about 5 m, which is explained by the constant length of fractures. The length variogram $\gamma_m(r)$ has relatively small values for small r, which indicates similarity of the lengths of close branches, with a range of correlation of 5 m. The combination of the information given by the two correlation functions yields the statement that close branches tend to be short and similar in length.

General

For the Artificial FN the second-order statistics of fractures well reflects the spatial behavior of a completely random collection of segments. This is shown by the pcfs, the mark correlation functions $k_{mm}(r)$ and mark variogram $\gamma_m(r)$. In contrast, the results for branches are more complex. There are spatial correlations, which result only from the construction of branches and their centers. It simply reveals that branch centers are randomly aligned on fractures randomly scattered in space.

In the following two examples sometimes a similar behavior will be observed, which would be hardly understood without knowledge of the results for the Artificial FN. Hence it may serve as a benchmark and an aid for interpretation.

5 Analysis of Two Natural FN

Two natural fracture patterns are studied in this paper. One presents fractures observed at large scale from a satellite image, which covers 120.000 m^2 of the southern flank of the Jabal Anhdar dome in the Oman Mountains. This FN has been widely studied because it can be considered as a typical example of those in large fractured carbonate reservoirs of the Middle East (Hilgers et al., 2006; Holland, Urai, et al., 2009; Holland, Saxena, & Urai, 2009; Gomez-Rivas et al., 2014). The map Figure 7 (a) used in this paper is taken from Zeeb et al. (2013) for comparison.

The other fracture pattern comes from the Hornelen basin in Norway. The original dataset consists of seven maps digitalized at several scales by Odling (1997). We focus our investigation on the one mapped by hand from an observation height of 4 m by Odling (1997). The map covers 324 m^2 (18×18 m, Figure 7 (b)) and describes a small-scale FN with a high number of small fractures. This is a typical joint pattern, which may be considered as an example of structures found in a non-stratabound massive rock (Odling et al., 1999).

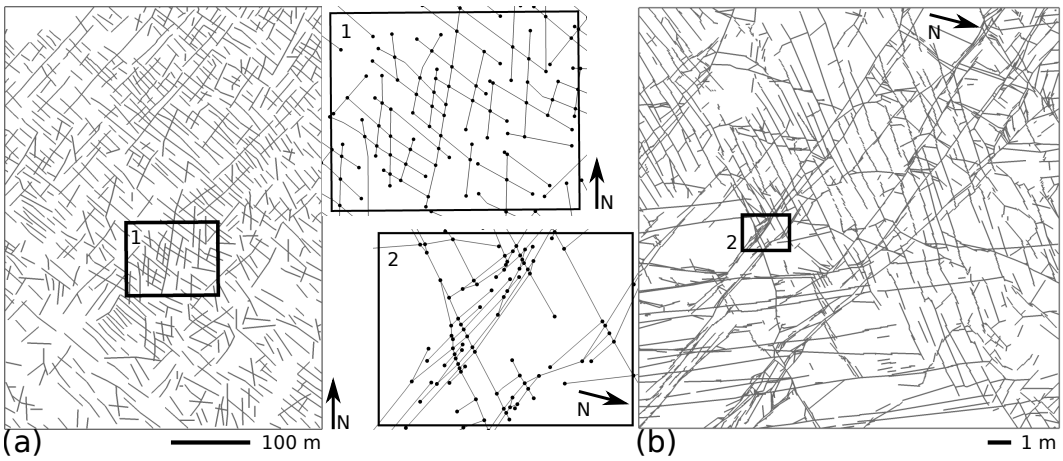

Figure 7. Natural surface exposures from (a) the southern flank of the Jabal Anhdar dome in the Oman Mountains (Zeeb et al., 2013) and (b) the Hornelen basin in Norway (Odling, 1997). The central part of the figure shows zoom of the central part of (1) the Oman dataset and (2) the Hornelen dataset. The I,V,Y, and X nodes are marked as black dots.

These datasets were chosen because of their complementary nature in terms of fracture pattern, scale, randomness, and variability. The Oman pattern has a spatially variable fracture density, which is a bit smaller in the lower part. The latter may be considered as a weak, but acceptable, deviation from homogeneity. For the Hornelen pattern, we decided to consider only sub-samples for the second-order analysis, since deviations from homogeneity turned out to be too strong. Of course, both patterns are clearly anisotropic.

Centers of fractures and branches were constructed by the median rule for segments not fully in the window of observation.

In the analysis, subsets of objects of similar orientation $\theta^c irc$ are considered, denoted as Nθ.

5.1 Statistics for the Oman Fracture Pattern

For the Oman fracture pattern, the map in Figure 7 (a)) was obtained by digitalization using the SKUA-GOCAD software. It was then analyzed by the first- and second-order methods of the present paper.

5.1.1 First-Order Characteristics

The Oman pattern has already been analyzed by Zeeb et al. (2013). Nevertheless, we studied the data again and we confess that we did not exactly obtain the same results. While there were originally 650 fracture traces with lengths ranging between 3 and 179 m, we found 696 fractures with lengths ranging between 1 and 134 m. Furthermore, while Zeeb et al. (2013) reported that approximately 5% of the sampled fractures appear to be cut by the boundary of the observation window, in our digitalization this rate is close to 7%. This illustrates some impact of subjective interpretation; there is some probability that other researchers would produce other maps from the same data.

For an unbiased estimation of the number of fractures, we counted 663 lower endpoints of fractures in the window of 120.000 m^2. This yields the estimate 5.6×10^{-3} m^{-2} of fracture density P_{20}. This value is comparable to the result one obtains when using the number of 650 traces reported by Zeeb et al. (2013).

Introducing branches increases the number of objects to 1476, and the lengths range now between 0.5 to 55 m. In parallel, the number of objects hitting the boundary is reduced to approximately 4%. Note that 40% of fractures are isolated (i.e., consisting of one branch bounded by two I-nodes), which means that 40% of the objects are the same in the fracture and branch representation. Segmentation of the other 60% of fractures leads to a density of 1.22×10^{-2} branches per square meter, which is 2.1 times more than for fractures.

The rose of directions (Figure 8 (b)) is computed by weighting object strike azimuths by the corresponding lengths. The result corresponds well to the given chequered pattern, which is strongly anisotropic with two (nearly) orthogonal main fracture sets of orientations 40° and 130°. The fractures associated to the direction 130° are quantitatively predominant. The rose of branch directions is quite similar to the one of the fractures; the small difference is caused by the approximation by segments.

The length distribution of objects was determined for both fractures and branches, see Figure 8 (a). Both distributions are asymmetric with medians clearly smaller than means. Additionally, Table 2 gives some information on the length distributions of the subsets N40 and N130. The mean fracture length of the set N40 is longer than that of N130, and the fractures of N40 are segmented more intensively. This is confirmed by a smaller mean and median of branch length distribution; and larger number of intersections per fracture C_f, which is 2.23 for N40 and 1.10 for N130.

Note that the union of the two sets N40 and N130 does not cover the complete fracture pattern as there exists a minor set with objects aligned to the North. It has been neglected as it contributes only to 10% of total length.

5.1.2 Second-Order Characteristics

Pair Correlation Functions: whole pattern

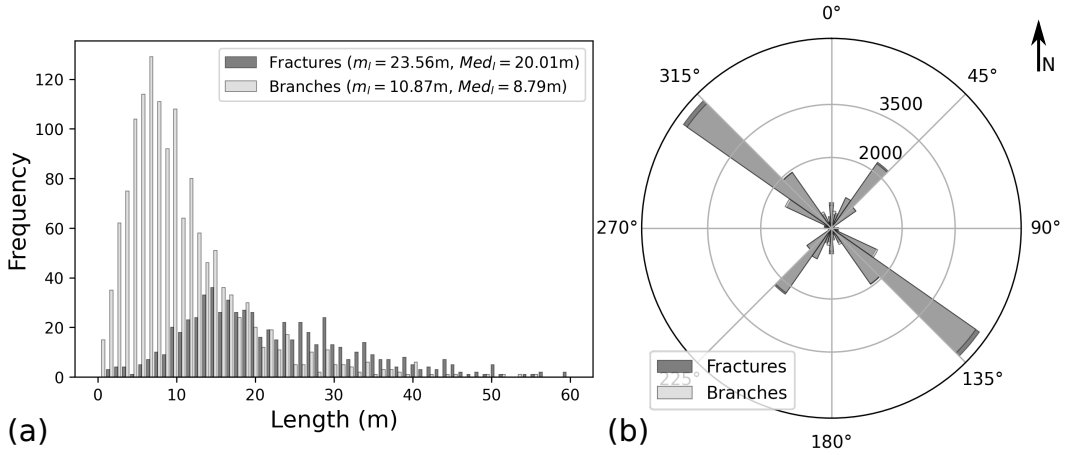

Figure 8. First-order characteristics of the Oman exposure, for fractures (black) and branches (gray). (a) Length distributions (values above 60 m are not plotted), (b) rose of strike azimuths weighted by length (per 10° interval).

Table 2. First-order characteristics of the Oman exposure

	Fractures			Branches		
	Full set	N40	N130	Full set	N40	N130
P_{20} (nb.m^{-2})	0.0056	0.0015	0.0035	0.0122	0.0045	0.0064
P_{21} (m^{-1})	0.132	0.041	0.078	0.132	0.041	0.078
mean length (m)	23.56	27.35	21.67	10.87	9.10	12.24
median length (m)	20.01	21.66	20.00	8.79	7.05	10.29
Connectivity						
C_f (nb.fracture^{-1})	1.42	2.23	1.11			
$p_{I-nodes}$	0.53	0.41	0.60			
$p_{Y-nodes}$	0.20	0.25	0.17			
$p_{X-nodes}$	0.27	0.34	0.24			

Figure 9 shows the empirical isotropic pcf and two anisotropic pcfs for the whole pattern of fractures and branches. The directions θ investigated for the anisotropic pcfs $g(r, \theta)$ are the two main orientations of objects 40° and 130°.

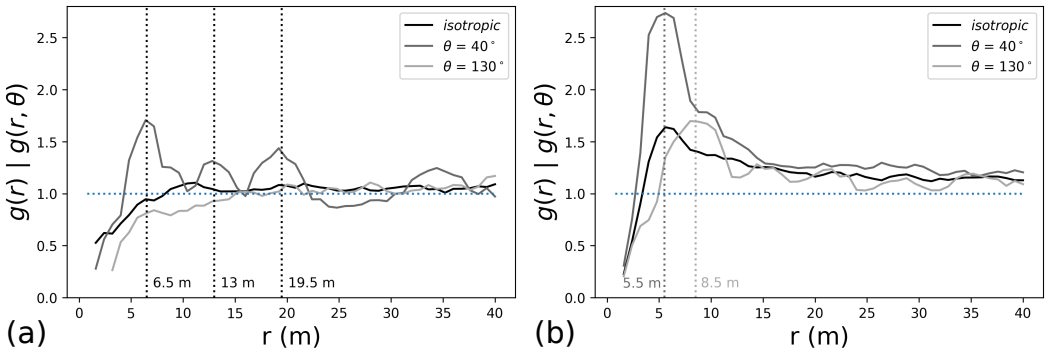

Figure 9. Isotropic pcf (black curve) and anisotropic pcfs (gray curves) for the full set of (a) fractures and (b) branches in the Oman dataset.

The pcfs for the fractures in Figure 9 (a) do not deviate largely from the value 1, which holds for the pcf in the case of complete spatial randomness of segment centers; the average of both directional pcfs is also close to the constant value of 1. However, the pcf for the direction 40° deviates a little. The maximum value at $r = 6.5$ m results from a number of similar inter-center distances close to 6.5 m. This particular shape indicates some short-range order (See Appendix C for explanation of the terms 'short-range order' and 'long-range order'.) There is even a second and a third maximum at $r = 13$ m and $r = 19.5$ m, which may be seen as a weak trace of long-range order, related to the visible nearly regular spacing of N130 fractures. Indeed, the pattern in Figure 7 (a) shows a lot of N130 fracture centers regularly aligned in the direction 40°.

The pcfs for the branches in Figure 9 (b) differ clearly from those for the fractures. They have the typical form of pcfs of point processes with short-range order: All possess a clear single maximum, which is around $r = 5.5$ m for the isotropic case and for the direction 40°, but around $r = 8.5$ m for the direction 130°.

This behavior can be explained by the chequered nature of the FN. A given fracture is typically intersected by other fractures, which are nearly orthogonal and these intersection points (which are the ends of branches) form nearly regular sequences. Consequently, the branch centers also form nearly regular sequences, which lead to the form of the pcfs. Since the intersection points do not form irregular sequences like in he Artificial FN (Section 4), there is no motive to think about a pole at $r = 0$. The r-value at the maximum gives information on typical (frequent) inter-point distances and on the size of the intact rock blocks. The differences in the values of the maxima of the pcfs (2.7 and 1.7) characterize the strength of order in each directions: branch centers are more regularly spaced in the direction N40 than in N130.

In order to obtain more detailed second-order information, we now refine the analysis by identifying the separate contributions of the sets N40 and N130 to the anisotropic pcfs.

Pair Correlation Function: Set N40

First we estimated isotropic and anisotropic pcfs for fractures and branches for the objects belonging to the set N40 (Figure 10). While the isotropic pcfs are close to the

typical form of complete spatial randomness, the anisotropic pcfs reflect interesting structure and reveal real differences in the spatial organization of fractures and branches.

In the direction 40°, the pcf $g(r, 40)$ for branches indicates a very high degree of short-range order by the maximum $g(r, 40) = 10.5$ at $r = 5.5$ m. (Note that the maximum value for the isotropic pcf for the whole pattern was clearly lower (2.7) but appeared at the same r value ($r = 5.5$m).) Perhaps there is even a second maximum at $r = 11$ m, which may show a trace of long-range order. This behavior reflects statistically the obvious order of arrangement in direction 40°, which is caused by the nearly equidistant intersections by the fractures of N130. That means, it reflects the order related to the nearly regular spacing between N130 fractures.

In contrast, $g(r, 40)$ for the fractures indicates repulsion until $r = 25$ m and disorder, there is no regular appearance.

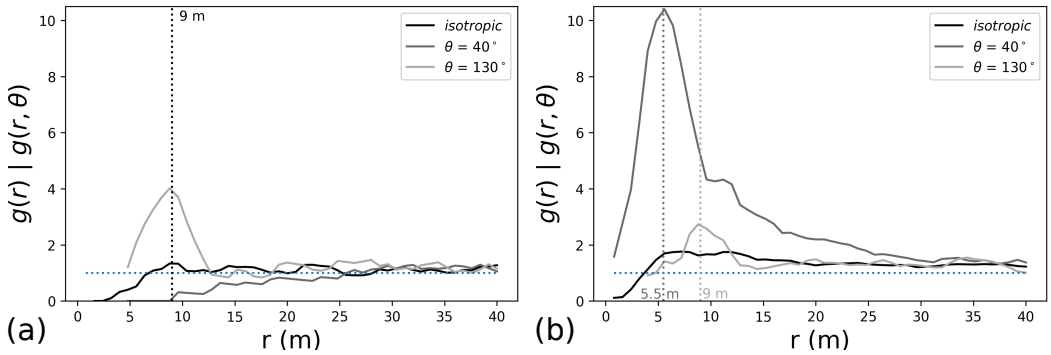

Figure 10. Empirical isotropic and anisotropic pcfs for (a) fractures and (b) branches of the subset N40 in the Oman dataset.

We remark that in the orthogonal direction 130°, the pcfs $g(r, 130)$ for fractures as well as for branches indicate weak short-range order (note the maximum at $r = 9$ m), i.e., they reflect the order related to the nearly regular spacing between N40 fractures.

Pair Correlation Function: Set N130

The pcfs corresponding to the subset N130 (Figure 11) have forms similar to those for the subset N40, but with lower values for the maxima. (Note the different scales at the ordinates in Figure 10 and 11.) In particular, the curves of $g(r, 130)$ for branches mark the difference well: There are maxima at $r = 7.5$ m and $r = 15$ m, but the values at the maxima are smaller (3.5 at $r = 7.5$ and 1.6 at $r = 15$ m). An interesting fact is that the curve for branches, also in the orthogonal direction (40°), indicates similar order with maximum values of 2 at $r = 7.5$ m and 1.5 at $r = 15$ m.

For fractures the curves of $g(r, 130)$ show repulsion between fracture centers ($g(r) < 1$) until $r = 22$ m and then irregular fluctuations around 1.

Finally, in the orthogonal direction 40°, the pcf $g(r, 40)$ for fractures indicates weak short-range order (indicated by the maxima at around $r = 6.5$ m), related to the nearly regular spacing between N130 fractures.

Pair Correlation Functions, Lengths and Spacing

For the Oman FN the analysis of branches yields interesting statements about the spatial distribution of the FN, while for the Artificial FN their role is questionable. In

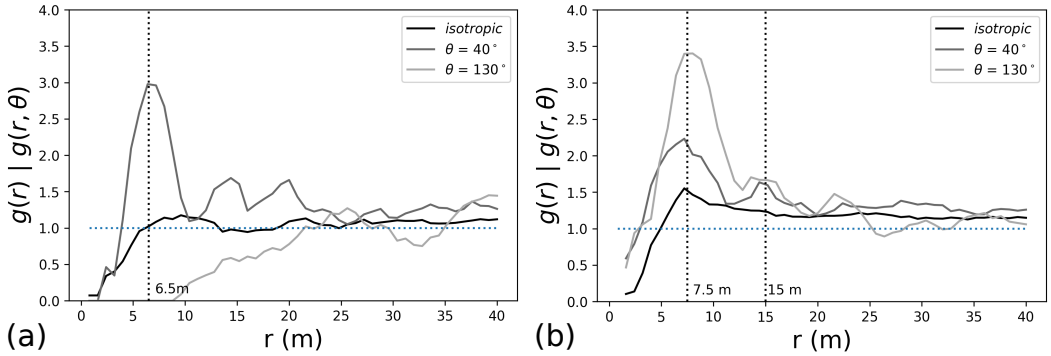

Figure 11. Empirical isotropic and anisotropic pcfs for (a) fractures and (b) branches of the subset N130 in the Oman dataset.

fact, the chequered nature of the FN causes that branches may be considered as its natural constituting elements.

The isotropic pcfs reveal little information about the spatial organization of the Oman FN. However, the anisotropic pcfs describe interesting aspects. In particular, the functions for the branches reflect the regularity caused by regular spacing between fractures of each sets.

A separate analysis of the N40 and N130 fracture set makes the statements even clearer: The r-values of the maxima of the pcfs for branches indicate very frequent interdistance between branch centers, which are slightly different according to the set considered and the direction investigated. The obtained forms are related to the length of branches and thus to their spacing. The higher degree of order shown in the direction 40° for branch centers of the N40 fracture set results from the long sequences of nearly regularly spaced branch centers. In fact, N40 fractures are quite long and also intensively segmented by N130 fractures, which are also regularly spaced.

Such a regularity is visible with fractures but only when considering pcfs in the direction perpendicular to fracture strike azimuth. Then, the spacing between fractures may be visible. On the contrary, there is some repulsion between fracture centers in the direction of object strike azimuth. This repulsion extends to the mean fracture length in each direction. This was expected as fractures of the same set cannot overlap because of the shadow zones around, see Darcel et al. (2003a).

Mark Correlation Functions and Variograms

Perhaps surprisingly, the empirical mark correlation functions and the mark variograms for fractures (Figure 12(a)) show a behavior similar to the Artificial FN (Figure 6(a)). If one ignores statistical fluctuations and deviations from the theoretical values in the case of independence (which result probably from deviations from homogeneity) they look as if they belong to independent length marks (Figure 12 (a)). This differs from a result of Bour (2002), who wrote "small faults are more clustered than large ones"[6]. Probably both situations may appear in nature, spatial correlations of fracture lengths and no-correlations [7] (Unfortunately, today statistical methods for proving significance statements in the context discussed are still missing.)

[6] In this case the mark correlations would look like the curve for fracture branches (Figure 12(b)).
[7] See also the mark correlation function for the Hornelen data in Figure 17.

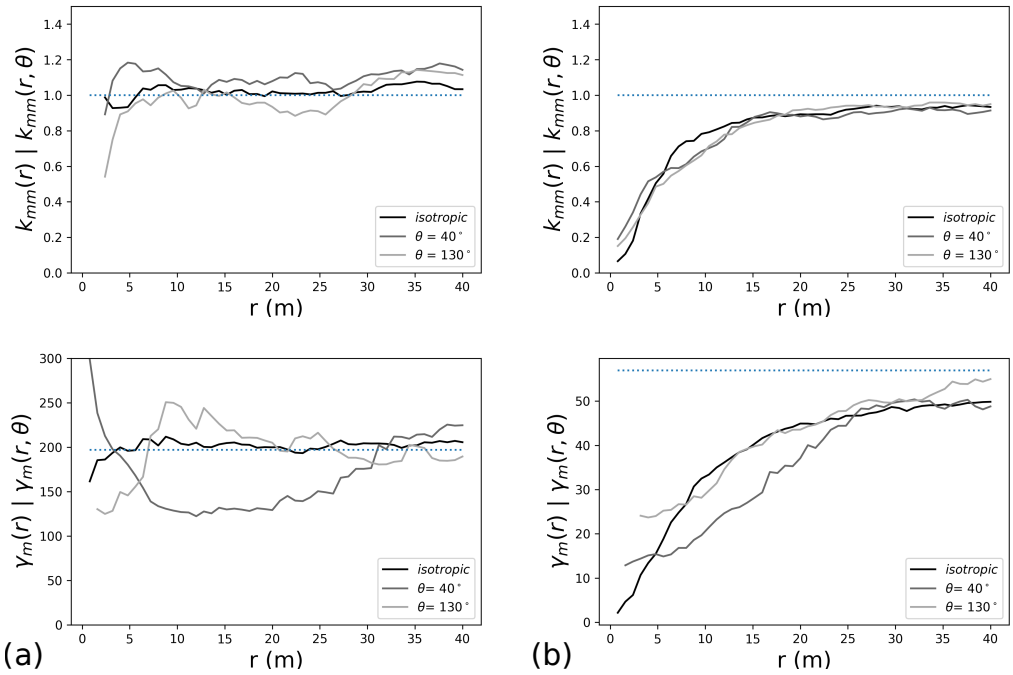

Figure 12. Empirical length-mark correlation function $k_{mm}(r)$ and length-mark variogram $\gamma_m(r)$ for (a) fractures and (b) branches of the Oman exposure. The theoretically expected values for large r or in case of independence are shown as dotted blue lines.

The empirical mark correlation functions $k_{mm}(r)$ for branches are shown in Figure 12 (b). They indicate spatial correlations of length marks that can be easily interpreted. For close branches the lengths tend to be smaller than the average length of branches, with a range of correlation of 30 m. (This is a clear difference to the case of fractures.) Also, the empirical length variograms $\gamma_m(r)$ shown in Figure 12 (b) indicate similarity of lengths for close branches, here again, with a range of correlation of 30 m. The combination of the information given by mark correlation function and mark variogram leads to the statement that close branches tend to be short and similar in length. This is plausible because of the construction of branches and the regularity of fracture spacing already described.

5.2 Statistics for the Hornelen Fracture Pattern

5.2.1 First-Order Characteristics

The map in Figure 7(b) contains 2109 fractures with lengths ranging between 1 cm and 11.0 m, 5.4% of fractures end on the boundary. Introducing the branch representation increases the number of objects to 4350 and reduces the range of object lengths (between 1.1 mm and 5.6 m) and the proportion of objects cut by the boundary to 2.6%.

We counted 2033 fracture lower end-points in the 324 m^2 window. This edge-corrected count yields the estimate 6.27 m^{-2} of P_{20}. 60% of the fractures are isolated and the segmentation of the other 40% lead to a density of 13.18 branches per square meter, which is almost twice the density of fractures.

The FN consists of three fracture sets oriented around 50°, 130°, and 170° . We mention a small difference to Odling (1997), who had for the third fracture set 0° when

considering all the seven maps. The rose of branch strike azimuths is, as expected, similar to that for the fractures (Figure 13 (b)).

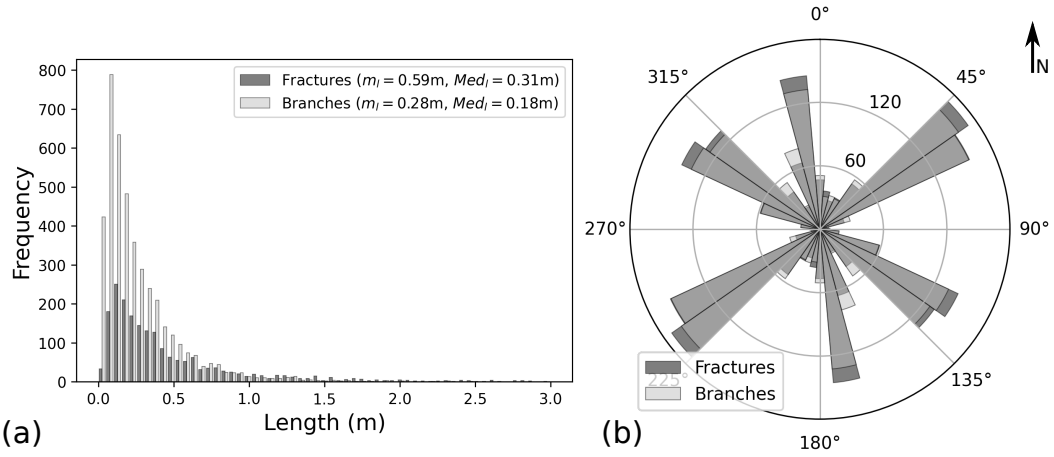

Figure 13. First-order characteristics of the Hornelen exposure, for fractures (black) and branches (gray). (a) Length distributions (values above 3 m are not plotted). (b) Roses of strike azimuths weighted by length (per 10° interval).

Here, we used the same statistical analysis as for the Oman data, this time for three sets of fractures, which we call N50, N130 and N170. As for Oman, a small part of the FN (9.6%) of the total length is not represented by these three subsets.

We learnt that when considering these sub-patterns (Figure 14 (a)) stronger deviations from homogeneity appear. Indeed the objects from the set N130 (green, Figure 14 (a)) have a higher density in the center of the exposure. Also, those from the set N170 (red, Figure 14 (a)) have a higher density in the South East of the exposure. Both sets have rather long fractures. In contrast, the set N50 (blue, Figure 14 (a)) is more diffuse and contains smaller and more isolated fractures. Therefore, we defined the sub-windows shown in Figure 14 (a) and made the statistical analysis, which assumes homogeneity, only for these smaller regions.

The empirical length distributions are asymmetric (Figure 13 (a)). This is consistent with the findings of Odling (1997), who fitted a lognormal distribution to the fracture lengths of this exposure. The length distributions of branches of the three sub-sets are presented in Table 3 and Figure 14 (b)).

The connectivity measures also reveal that the average number of connections per fracture of the set N130 is higher than for the sets N50 and N170. The high number of small fractures in the set N50 may be an explanation for its low connectivity index.

5.2.2 Second-Order Characteristics

Pair Correlation Functions: whole pattern

The Hornelen FN is characterized by the empirical isotropic and anisotropic pcfs (Figure 15). The directions are those defining the three fracture sets, 50°, 130° and 170°.

The isotropic pcf for fracture centers indicates weak short-range order with a most frequent inter-center distance of 0.08 m. There is no reason to think of a pole at $r = 0$. For the anisotropic pcfs with $\theta = 50°$ and 130°, we note a weak long-range order re-

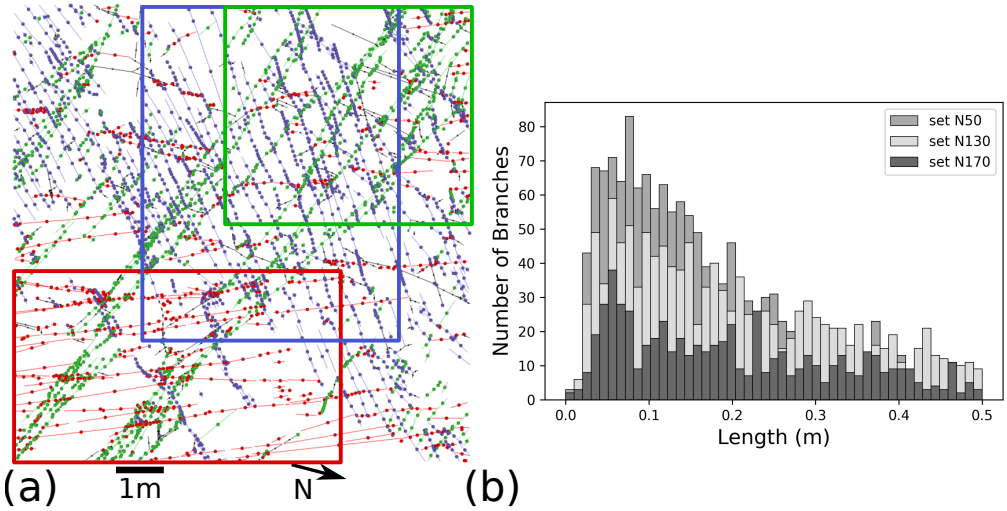

Figure 14. Hornelen surface exposure: (a) Map of the branch centers, N50 (blue), N130 (green), N170 (red), and rest in black. Statistical analysis for these sets is carried out for the three identified sub-regions. (b) Length distributions, N50 (dark gray), N130 (light gray), and N170 (black). The focus is on objects that have a length ranging between 0 and 0.5 m.

Table 3. Hornelen first-order characteristics

	Fractures				Branches			
	Full set	N50[a]	N130[a]	N170[a]	Full set	N50[a]	N130[a]	N170[a]
P_{20} (nb.m^{-2})	6.27	3.23	1.76	1.63	13.20	6.32	5.65	3.89
P_{21} (m^{-1})	3.68	1.50	1.43	1.72	3.69	1.51	1.44	1.72
mean length (m)	0.59	0.47	0.82	1.05	0.28	0.24	0.26	0.44
median length (m)	0.31	0.23	0.43	0.37	0.18	0.16	0.19	0.23
Connectivity								
C_f (nb.fracture^{-1})	1.76	1.16	2.62	1.92				
$p_{I-nodes}$	0.42	0.59	0.34	0.40				
$p_{Y-nodes}$	0.41	0.26	0.46	0.37				
$p_{X-nodes}$	0.17	0.15	0.20	0.23				

[a] Statistics for each subset are made on the sub-regions identified in Figure 14 (a).

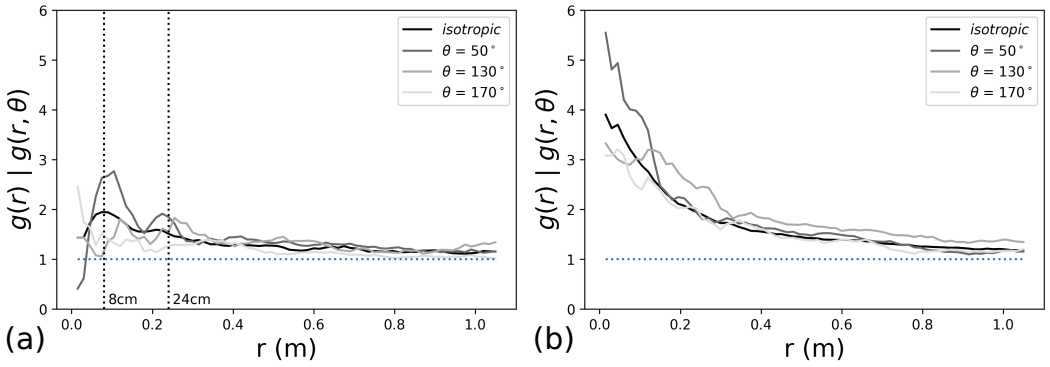

Figure 15. Isotropic pcf (black curve) and anisotropic pcfs (gray curves) for the full set of fractures (a) and full set of branches (b) of the Hornelen exposure.

spectively with maxima at $r = 0.08$ and 0.24 m for $\theta = 50°$, and at $r = 0.12$ and 0.24 m for $\theta = 130°$. For $\theta = 170°$ the pcf indicates complete spatial randomness.

For the branches, the pcfs indicate some form of clustering. The situation here is similar to the one for the Artificial FN.

Pair Correlation Function: Subsets

We now present empirical isotropic and anisotropic pcfs for the subsets N50, N130, and N170 separately. As we did for the Oman dataset, we investigate for anisotropic pcfs the direction defined by the object strike azimuths (dark gray curves Figure 16) and the perpendicular direction (light gray curves Figure 16).

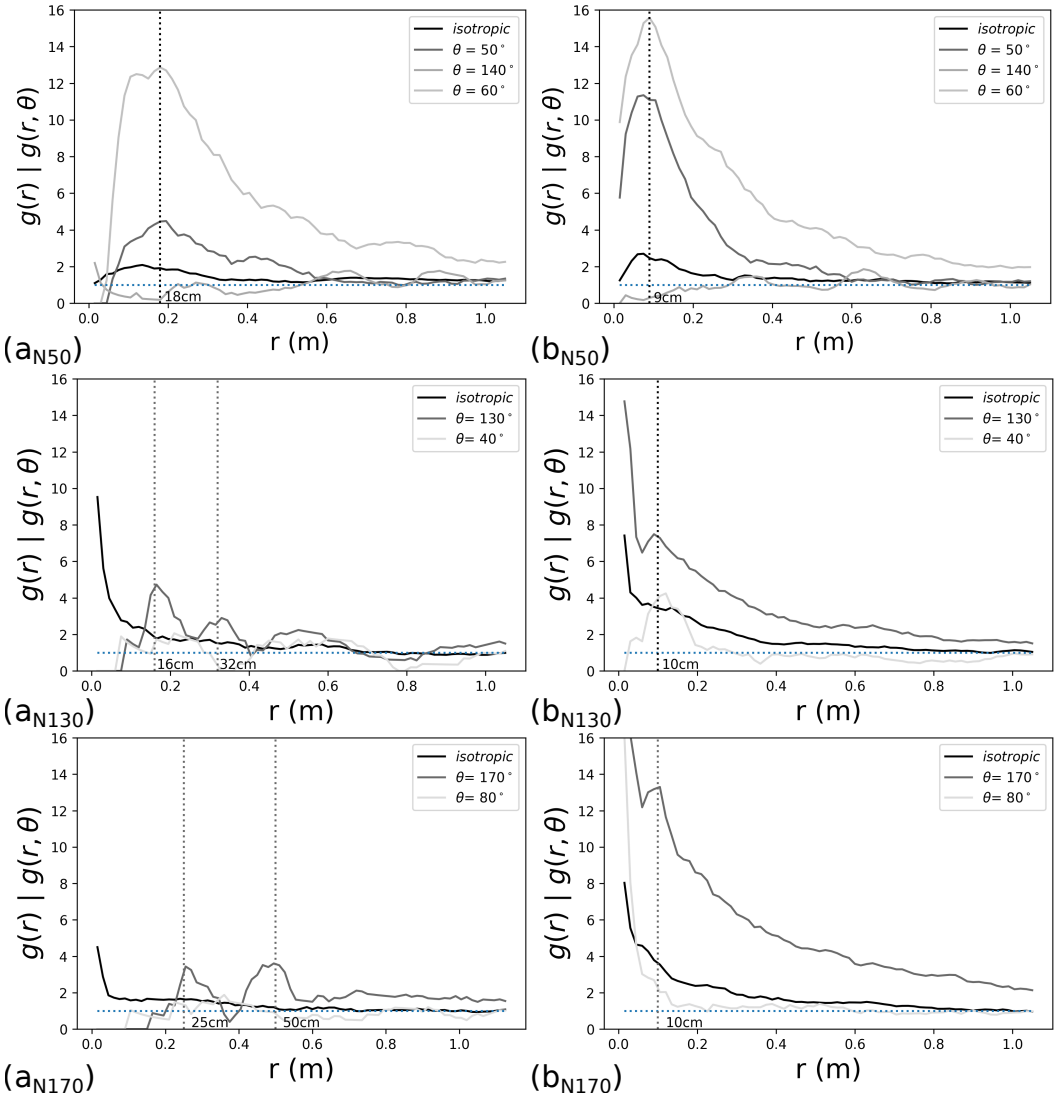

Figure 16. Empirical isotropic and anisotropic pcfs for (a) fractures and (b) branches of the subsets N50, N130 and N170 in the Hornelen dataset.

For fractures of the two sets N130 and N170, there are some similarities in their organization. The anisotropic pcfs in the direction of objects indicate some weak long-range order with two maxima at $r = 0.16$ and 0.32 m for $\theta = 130°$ (Figure 16 (a_{N130})),

and at 0.25 and 0.5 m for $\theta = 170°$ (Figure 16 (a_{N170})). For the set N50, the 50° anisotropic pcf indicates some short-range order with most frequent inter-center distance $r = 0.18$ m. In all cases, irregularity is shown in the direction perpendicular to objects.

For this last set N50, because of en-echelon structures, we observed that many segment centers are aligned in the direction $\theta = 60°$. Therefore, we investigated additionally this extra direction. The corresponding curve (for $g(r, 60)$, not shown) has a similar shape as for $\theta = 50°$, but with higher short-range order (Figure 16 (a_{N50})). This reveals the dominance of en-echelon fractures for this set.

For the branches, the pcf curves for both the N130 and N170 subsets indicate clustering of centers. The situation looks like the one observed and explained for the Artificial FN. The degree of clustering is obviously higher here, because the branch centers on the fracture traces are even clustered (Figure 7(b)) and not (Poisson-process-like) random as with the Artificial FN.

The curves for the branches of the N50 fracture set show short-range order with a very high maximum value of the pcf at $r = 0.09$ m in both directions 50° and 60°. It reflects a very probable inter-point distance of 0.09 m, which is half of the value measured on the pcf for N50 fractures. This is in line with the connectivity index of 1.13 intersections per fracture (Table 3) which suggests that N50 fractures are often divided into two pieces. Also, an inspection of Figure 14(a) reveals that N50 fractures (in blue) are typically intersected by N130 fractures (in green). And, considering N130 fracture branches, the 40° pcf (i.e. perpendicular to objects) also shows some short range order with a maximum at $r = 0.10$ m. Thus, the spacing of the fractures of the set N130 is related to the segmentation of N50 fractures.

Mark Correlation Functions and Variograms

The empirical isotropic and anisotropic mark correlation functions and variograms for the branches of the Hornelen dataset in Figure 17 reveal a similar form of spatial correlation as with Oman (Figure 12), of course with quite different length scales and ranges of correlation.

For the fractures, the Oman results are closer to a behavior expected for randomness, while with Hornelen there is some inhibition of lengths at short distances (upto 0.6 m), and the mark variogram indicates some tendency of similarity of lengths upto 0.5 m. The combination of information given by the two correlation functions yields the statement that close fractures and branches tend to be short and similar in length.

More precisely: Consider a randomly chosen pair of fractures with a distance r between their centers, denote by l_1 and l_2 the lengths of these fractures. Let the mean of the product $l_1 \cdot l_2$ be $m(l_1 l_2)$, while the mean fracture length in the FN is m_l. Then

$$k_{mm}(r) = \frac{m(l_1 l_2)}{m_l^2}. \tag{7}$$

The curves in Figure 17(a) for $k_{mm}(r)$ can be approximated by

$$k_{mm}(r) = 0.2 + \sqrt{r} \text{ for } r \leq 0.6 \text{ m} \tag{8}$$

and $k_{mm}(r) = 1$ for $r > 0.6$ m. This shows that close fractures (closer than 0.6 m) tend to be shorter than the average in the FN, since the mean of the corresponding lengths is smaller than the square of total mean length.

This result may be compared with findings in Darcel et al. (2003a), where nearest-neighbor correlations[8] were studied on the seven maps of the Hornelen dataset. The main

[8] This statistical approach is an alternative to second-order methods.

finding is: The average distance $d_c(l)$ between the center of a fracture of length l to its nearest-neighbor fracture center depends weakly on l, it is $d_c(l) \sim l^{0.3}$ for small l, but is independent for larger l, as expected for independent length marks.

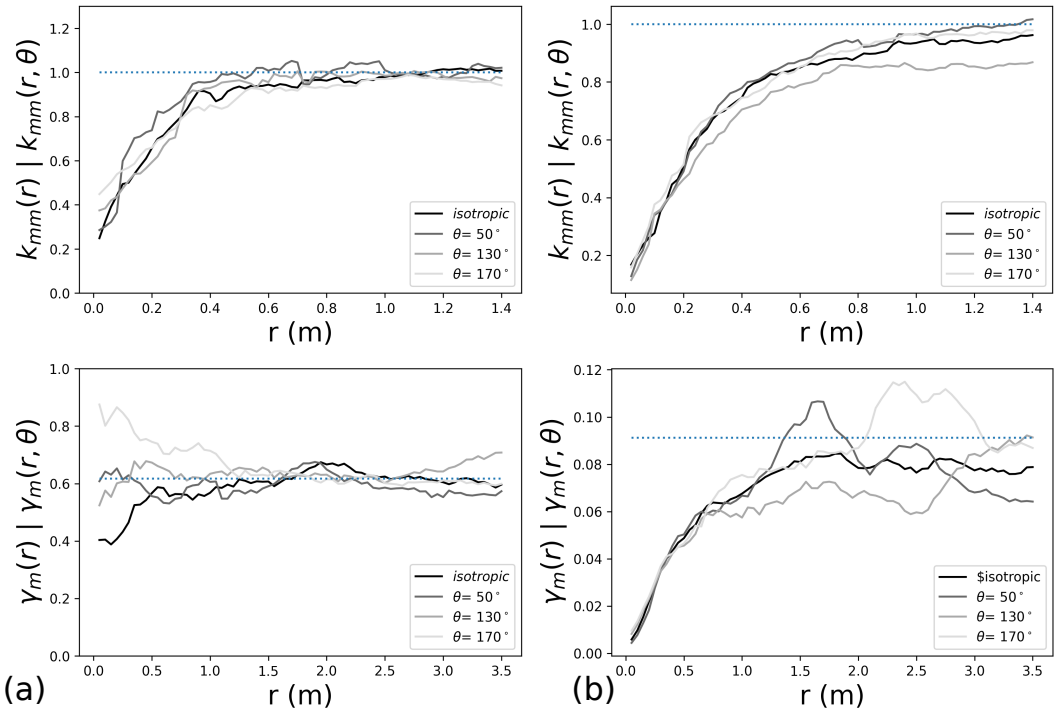

Figure 17. Empirical length-mark correlation function $k_{mm}(r)$ and length-mark variogram $\gamma_m(r)$ for (a) fractures and (b) branches of the Hornelen outcrop. The theoretically expected values for large r are shown as dotted blue lines.

5.3 Comparison of the Oman and Hornelen FN

The analysis in the Sections 5.1 and 5.2 shows clear differences in various senses between the two FN. While the Oman FN is clearly anisotropic, with two dominating directions, almost perpendicular, the Hornelen FN shows directional disorder with perhaps three main directions. The pattern shows so much variability that we had to consider three sub-samples for an acceptable second-order analysis. There is some similarity to the Artificial FN, however with higher local variability: While for the Artificial FN the branch centers form pieces of samples of one-dimensional Poisson processes, they show even clustering for the Hornelen FN.

In short, the Oman FN is a well developed chequered pattern with long fractures, highly connected and regularly spaced. Thus, most of its fractures (60%) are composed of series of branches. The Hornelen FN is composed of a lot of small fractures (60%) aligned and almost connected. There is a development and a connection of aligned (en-echelon) fractures, where probably larger fractures drive the development of smaller ones at their tips. These observations are refined and quantified by the second-order analysis.

For the Oman FN the fractures of the N130 set contribute more to the total fracture length than those of the N40 set. Also, the anisotropic pcfs show that N130 fractures are more regularly spaced than N40 fractures. For both directions (40° and 130°) there is short-range and partially even long-range order, in a weaker extent for the di-

rection 40°. The maxima of the pcfs are at positions (r-values) determined by the modes of branch lengths, as it is to expect because of the chequered nature of the FN. The analysis of branches yielded a clearer information than the analysis of fractures.

For the Hornelen FN there is disorder in a great extent: We could not identify a direction that really dominates the FN. The sets N130 and N170 show some degree of long-range order (in their sub-windows), while N50 seems to reveal only some short-range order. The N50 fracture centers are not well aligned to fracture azimuths (Figure 5 (a_{N50})), most likely because of a large proportion of en-echelon fractures. In contrast to the Oman FN, here the fractures seem to be the more interesting objects in the second-order analysis.

6 Discussion

When we started our research for this paper, we assumed that the isotropic pair correlation function $g(r)$ was a suitable tool for second-order analysis of FN by point-process methods. Discussions with colleagues and own experience taught us that orientations play a very important role in such a statistical analysis. We are now convinced that the anisotropic pcf $g(r, \theta)$ is the crucial tool to for quantitative description of the inner organization of fractures and fracture branches.

This paper uses the marked-point-process approach taking both fractures and branches as marks standing for individual linear segment. This implies that we consider objects as separate units, as marked points–so we keep the interpretation of fracture and there is no loss of information.

The 'points' in this paper, as well as in the literature we know, are geometrically defined as object centers. However, the ideal choice would be points that determine fractures in a physical sense such as nucleation points. Unfortunately, such points do not make sense for planar samples, and in three-dimensional samples their detection seems to be hopelessly complicated. Therefore, for fracture statistics with point-process methods the use of centers seems to be appropriate.

An important question in the statistical characterization of FN is: Which objects should be used: fractures or branches? On the one hand, fractures are the primary objects of an FN as they hold the geological interpretation that may reveal some inner organization. However, fractures may be rather long and their centers may have little to do with their full appearance. This is particularly true if their lengths span over several orders of magnitude. On the other hand, branches are only secondary objects as they subdivide fractures according to their intersections. However, branches have some topological meaning and capture information about connectivity of FN. Also, the range in their length distributions is reduced in comparison to fractures. Therefore, the use of branches may sometimes be a good compromise in variability and correlation analysis.

In a concrete application, it probably makes sense to study fractures and branches in parallel, until some tendency in the data helps to decide. For instance, if the FN is well developed and highly connected, branches may be considered as its main constitutive elements and yield the more interesting information. But if the FN contains a lot of isolated fractures (e.g. en-echelon), their analysis may be clearer if branches are not considered. The Hornelen dataset is a composition of both long interconnected and small isolated fractures. These are different configurations that may call for separate analysis in order to better understand the transition between 'poorly-developed' FN (also known as 'unsaturated' or 'dilute') and "well-developed" FN (also known as 'saturated' or 'dense') (Wu & D. Pollard, 1995; Josnin et al., 2002; Davy et al., 2010).

Relations such as equation (8) and its nearest-neighbor counterpart are probably valid only for special FN. Only further research for many various FN may lead to general results and a deeper understanding.

In the definition of fracture branches, nodes are of particular interest. Indeed, the nodes contain vital information (1) about the relationship between fractures (abutting/cross-cutting), (2) about potential stress concentration and interaction and (3) on relative timing of fractures. This even remains true in the planar case. Systematic studies of node-related statistics may be aims for the future.

Several times in this paper, we have mentioned an alternative approach that uses ideas from the theory of segment processes as in Chiu et al. (2013), chapter 8, and Stoyan (2021). In this context, the whole FN is considered as a sample of a random collection of one-dimensional objects, in particular straight-line segments. In contrast to the object-system approach the individual segments are not considered, only their contribution to the planar distribution of total segment length. Then, one is free of the need to define individual object, i.e. 'points'. The fracture intensity P_{21} and the rose of directions are characteristics of a long tradition, which can be seen as belonging to the segment-process approach. The systematic use of segment processes could be an alternative approach in FN statistics in future. Here we do not recommend it because of difficulties in the corresponding second-order theory, which are sketched around page 330 in Chiu et al. (2013): The segment-process analogue of the pair-correlation function has always a pole at $r = 0$, which makes fine analyses difficult.

Obviously, the Boolean segment process with Poisson-process centers is a model too simple for realistic stochastic modeling of FN. Nevertheless, our results for the Oman FN as well as for the Hornelen FN show that better models should be searched in 'the neighborhood' of the Boolean process. The pcfs of fracture centers in the Figures 9(a) and 15(a) are not very far from the simple form $g(r) \equiv 1$ true for a Poisson process. Perhaps realistic models may be obtained with other point processes.

7 Conclusions

Advanced methods of statistics for planar point processes lead to a quantitative description of variability and inner correlations of FN. The paper presents, in a rigorous and accessible way, the tools for such analyses. They are based on constructed marked points that stand for fractures or fracture branches, also called 'objects'.

There is no a-priori criterion for the decision to work with fractures or fracture branches. However, the degree of connectivity of fractures and the proportion of isolated fractures may help to decide. A safe recommendation is to use both variants in parallel for the same FN because of the complementary of the information obtained. The study of fractures leads to a quantitative description of their hierarchical organization, while an analysis based on branches describes fracture spacing and segmentation.

A key idea is the use of the anisotropic pair correlation function for analysis of inner correlations of subsets of objects. In the present paper, the subsets consist of objects of similar orientation, which introduces strong directionality into the statistical analysis, which is indispensable in FN statistics. However, different rules for forming subsets may be considered and other subsets may be analyzed in the future.

The application of second-order analysis to the simple Artificial FN, a Poisson-Boolean segment process, tests the methods under ideal conditions. It helps to understand the results for more complicated cases and serves as a benchmark, which describes results in the case of complete randomness. The analysis of the two natural FN shows clear deviations from that ideal case, which, however, explains finer aspects.

Application of the presented statistical methods for a large number of surface exposure patterns may be of value for better understanding and classification of FN. FN are not always so different as the two natural FN considered here, thus also finer differences may be be detected and measured.

Finally, information gathered by the presented statistical method opens the path to better mathematical models for stochastic simulations of FN. At least, it may be used to test the quality of stochastic models of three-dimensional FN by analyzing some of their planar sections.

Appendix A The Miles-Lantuejoul Estimator

The Miles-Lantuejoul sampling method is a general estimation principle in spatial statistics, created by Miles (1974) and Lantuéjoul (1978). It is applicable to planar and spatial systems of objects randomly distributed for estimating quantities describing their size distribution. The structure is assumed to be homogeneous.

The basic idea is minus-sampling: The objects can be observed only in a window W and objects only partly inside are ignored. There is some trick of weighting the observations so that one is close to unbiased estimation. Of course, the method has no magic power to use information from very large objects. (By the way, there is also a method called 'plus-sampling', which assumes that all objects in the window W and all objects hit by W can be measured completely.)

Here we explain the Miles-Lantuejoul estimator for the case of segments in the plane. The aim is to estimate a histogram of segment lengths. We consider the bin $[l_k, l_{k+1}]$. The window is a rectangle with sides parallel to x- and y-axis of lengths a and b.

The total number of lower segment end-points in W is denoted by N. Only segments fully in W are measured, their number is denoted by n. The segments are described as follows: The reference points are the lower end-points, the segment lengths are denoted by L_i for $i = 1, 2, \ldots, n$. The orientation of segment i is described by the rectangle with sides parallel to x- and y-axis having the segment as diagonal, with side lengths x_i and y_i. (If the segment is parallel to x-axis (y-axis), then $x_i = L_i$ and $y_i = 0$ ($y_i = L_i$ and $x_i = 0$).

The estimator of the probability p_k that segment length is in the bin $[l_k, l_{k+1}]$ is

$$p_k = \frac{ab}{N} \sum_{i=1}^{n} \frac{\delta_{ki}}{(a - x_i)(b - y_i)} \tag{A1}$$

with

$$\delta_{ki} = 1 \text{ if } l_k \le L_i < l_{k+1} \text{ and } = 0 \text{ otherwise.} \tag{A2}$$

Appendix B Estimating Pair Correlation Functions and the Role of Band-Widths

This paper uses extensively statistics for pair correlation functions. This appendix explains some of the main ideas of the estimators used. Kernel estimators are used in order to obtain smooth curves for empirical pcfs. The degree of smoothness obtained depends on the choice of a 'band-width' h, which determines the region around a distance r which is used to estimate $g(r)$. While estimators of the isotropic $g(r)$ and of the mark correlation functions are available in the statistical software R and explained in detail in Illian et al. (2008) and Baddeley et al. (2016), here the anisotropic pcf $g(r, \theta)$ is in the focus.

The basic idea is to analyze inter-point distances of point pairs. For estimating $g(r, \theta)$ only point-pairs that determine lines of an azimuth direction $\theta \pm \delta$ are considered; they

are called "θ-pairs". In this paper, we work with $\delta = 5°$. The arc of $\theta \pm \delta$ is denoted by α; its numerical value is $\frac{10}{180}\pi$.

These distances are collected to obtain groups of point-pairs of an approximate inter-point distance r. The collection is made with a "kernel function". The simplest case, which is also used in the paper, is the "box kernel": All point-pairs of a distance between $r-h$ and $r+h$ are included with equal weight $1/2h$. The actual distance value between points is ignored, and h, a positive parameter, is called the "band-width".

The band-width h has great influence on the results: With a large h the curves obtained are smooth, fine details are smoothed away. In contrast, with a small h the curves become spiky. The optimal choice of h is an art. A simple receipt is to start with

$$h = \frac{0.1}{\sqrt{P_{20}}}$$

and then search by experimentation for a good h. The aim is to obtain smooth curves that show nevertheless interesting details. Values for h used in this paper are either constant or adapted, i.e. piece-wise constant and increasing with r. In the latter case, we use the notation $(h_{r\le r_t}, h_{r>r_t}, r_t)$. The Table B1 presents all values of band-width used in this paper.

There are also other kernels, which give distances closer to r more weight than to others.

The estimator of the anisotropic pair correlation function $g(r,\theta)$ is

$$\hat{g}(r,\theta) = \sum_{(x_i,x_j)\in(r,\theta)} \frac{1}{2h\cdot\alpha\cdot r\cdot(A-a_{ij})\cdot(B-b_{ij})}/\lambda^2, \tag{B1}$$

where x_i and x_j are fracture (or branch) centers and the summation goes over all θ-pairs with an inter-point distance between $r-h$ and $r+h$. The window of observation W is a rectangle with side-lengths A and B in x- and y-direction, respectively. The absolute value of the x-component of x_i-x_j is a_{ij}, and b_{ij} is the same with for the y-component. The term $(A-a_{ij})(B-b_{ij})$ replaces the simpler $a = AB$, the window area, in order to make an edge-correction.

Finally, λ is the same as P_{20}, fracture density in the case of fracture centers, either of all centers or all centers of a subset Nθ; and analogously in the case of branches.

Appendix C Short-Range and Long-Range Order

The terms 'short-range order' and 'long-range order' have their origin in physics and chemistry in the context of atomic patterns. In this paper, they are used in a slightly modified meaning in the hope to make them useful for spatial statistics in geological applications.

The term 'long-range order' is in full agreement with the classical wording, if applied to a lattice of points. For a quadratic lattice with side length a the pcf has poles at $r = a$, $r = \sqrt{2}a$ and $r = 2a$ etc. When the points are slightly randomly moved, the pcf would have maxima at these values of r.

In geological contexts, with scales suitable for fractures, such patterns are non-typical. Already a sequence of two maxima of a pcf at some r-values a and $\sqrt{2}a$ are somewhat remarkable. In such cases, we use the term 'long-range order'.

If there is at least a clear maximum of a pcf at some r-value, this marks a clear difference to patterns of complete randomness belonging to a Poisson process, the pcf of which does not have any maximum. In order to show that this is somewhat remarkable, we use here the term 'short-range order'.

Table B1. Band-widths h (in m) for the figures

Figure	h_{iso}	h_θ
4 (a)	0.35	0°:0.35 ; 90°:0.35 ; 130°:0.35
4 (b)	0.15	0°:0.4; 90°:0.4 ; 130°:0.4
5 (a)	0.3	0°:0.7 ; 90°:0.7
5 (b)	0.2	0°:0.35 ; 90°:0.35
6 (a) k_{mm}	0.35	0°:0.35 ; 90°:0.35 ; 130°:0.35
6 (a) γ_{mm}	0.35	0°:0.35 ; 90°:0.35 ; 130°:0.35
6 (b) k_{mm}	0.4	0°:0.8 ; 90°:0.95 ; 130°:0.8
6 (b) γ_{mm}	0.45	0°:0.9 ; 90°:0.9 ; 130°:0.9
9 (a)	(1.8,1.9,16)	40°:(1.8,2.6,16) ; 130°:(1.9,5,8.8)
9 (b)	(0.8,1.0,8)	40°:(1.,2.9,12.8) ; 130°:(1.5,1.8,14.4)
10 (a)	2	40°:(4,7,12) ; 130°:(2.,5,14.4)
10 (b)	1.5	40°:(1.9,4,12) ; 130°:(2,2.7,14.4)
11 (a)	2	40°:(1.9,3.6,22.4) ; 130°:(2.6,3.2,14.4)
11 (b)	(0.8,1.4,8)	40°:(1.9,3.5,16.8) ; 130°:(1.6,2,20)
12 (a) k_{mm}	(2.7,3.6,16)	40°:(5,6.5,14.4) ; 130°:(5,6.5,5.6)
12 (a) γ_{mm}	(5.5,9.5,6.4)	40°:(7,14.5,7.2) ; 130°:(5,12,8.0)
12 (b) k_{mm}	(1,3,8.0)	40°:(4,6,19.2) ; 130°:(5,10,12.8)
12 (b) γ_{mm}	(2,4,9.6)	40°:(4.5,6,19.2) ; 130°:(6,10,12.8)
15 (a)	0.03	50°:(0.035,0.08,0.33) ; 130°:(0.03,0.08,0.33) ; 170°:(0.07,0.1,0.33)
15 (b)	0.027	50°:(0.027,0.05,0.33) ; 130°:(0.027,0.05,0.33) ; 170°:(0.027,0.05,0.33)
16 (a_{N50})	0.06	50°:(0.05,0.085,0.09) ; 140°:0.06 ; 60°:(0.035,0.089,0.09)
16 (b_{N50})	0.02	50°:(0.03,0.045,0.075) ; 140°:0.04 ; 60°:(0.035,0.05,0.3)
16 (a_{N130})	0.07	40°:(0.07,0.11,0.6) ; 130°:(0.07,0.11,0.6)
16 (b_{N130})	0.03	40°:(0.05,0.1,0.3) ; 130°:(0.05,0.1,0.3)
16 (a_{N170})	0.07	80°:(0.07,0.15,0.6) ; 170°:(0.07,0.15,0.6)
16 (b_{N170})	0.04	80°:(0.04,0.1,0.15) ; 170°:(0.04,0.1,0.15)
17 (a) k_{mm}	(0.09,0.2,0.7)	50°:(0.35,0.55,0.7) ; 130°:(0.35,0.55,0.7) ; 170°:(0.35,0.55,0.7)
17 (a) γ_{mm}	0.15	50°:0.6 ; 130°:0.6 ; 170°:0.6
17 (b) k_{mm}	(0.027,0.08,0.4)	50°:(0.1,0.25,0.4) ; 130°:(0.1,0.25,0.4) ; 170°:(0.1,0.25,0.4)
17 (b) γ_{mm}	0.075	50°:(0.09,0.2,0.7) ; 130°:(0.09,0.2,0.7) ; 170°:(0.09,0.2,0.7)

When describing short-range and long-range order the r-values at the maxima are important because they indicate frequent inter-point distances. Also the maximum values are important, since they characterize the relative frequency of these distances.

Acknowledgments

This work was performed in the frame of the RING project (http://ring.georessources.univ-lorraine.fr/) at Université de Lorraine. We acknowledge support from the industrial and academic sponsors of the RING-GOCAD Consortium managed by ASGA.

All the data used in this paper has already been published in the literature. We thank Conny Zeeb and Noelle Odling for providing us the data for the two natural FN.

We are grateful to Gautier Laurent and Guillaume Caumon for their constructive remarks; and to the reviewers David J. Sanderson and Tom Manzocchi. In addition, we thank the associate editor Isabelle Manighetti for encouraging us to make the extensive revision of the original manuscript.

Finally, we are thankful to Emerson for the SKUA-Gocad Software and development kit; and Geode-solutions for the OpenGeode plateform.

References

Agterberg, F. (2014). *Geomathematics: theoretical foundations, applications and future developments*. New York: Springer.

Baddeley, A., Rubak, E., & Turner, R. (2016). *Spatial point patterns: methodology and applications with R*. Boca Raton ; London ; New York: CRC Press, Taylor & Francis Group. (OCLC: ocn933300812)

Balberg, I., & Binenbaum, N. (1983). Computer study of the percolation threshold in a two-dimensional anisotropic system of conducting sticks. *Physical Review B*, *28*(7), 3799–3812. doi: 10.1103/PhysRevB.28.3799

Bergbauer, S., & Pollard, D. D. (2004). A new conceptual fold-fracture model including prefolding joints, based on the Emigrant Gap anticline, Wyoming. *Geological Society of America Bulletin*, *116*(3), 294. doi: 10.1130/B25225.1

Berkowitz, B. (1995). Analysis of fracture network connectivity using percolation theory. *Mathematical Geology*, *27*(4), 467–483. Retrieved 2021-08-19, from `http://link.springer.com/10.1007/BF02084422` doi: 10.1007/BF02084422

Bistacchi, A., Mittempergher, S., Martinelli, M., & Storti, F. (2020). On a new robust workflow for the statistical and spatial analysis of fracture data collected with scanlines (or the importance of stationarity). *Solid Earth*, *11*(6), 18. doi: 10.5194/se-2020-83

Bonneau, F., Caumon, G., & Renard, P. (2016). Impact of a stochastic sequential initiation of fractures on the spatial correlations and connectivity of discrete fracture networks: stochastic sequential DFN simulation. *Journal of Geophysical Research: Solid Earth*, *121*(8), 5641–5658. doi: 10.1002/2015JB012451

Bonnet, E., Bour, O., Odling, N. E., Davy, P., Main, I., Cowie, P., & Berkowitz, B. (2001). Scaling of fracture systems in geological media. *Reviews of Geophysics*, *39*(3), 347–383.

Bour, O. (2002). A statistical scaling model for fracture network geometry, with validation on a multiscale mapping of a joint network (Hornelen Basin, Norway). *Journal of Geophysical Research*, *107*(B6), 2113. doi: 10.1029/2001JB000176

Cherpeau, N., & Caumon, G. (2015). Stochastic structural modelling in sparse data situations. *Petroleum Geoscience*, *21*(4), 233–247. doi: 10.1144/petgeo2013-030

Cherpeau, N., Caumon, G., & Lévy, B. (2010). Stochastic simulation of fault

networks from 2D seismic lines. In *SEG Technical Program Expanded Abstracts 2010* (pp. 2366–2370). Society of Exploration Geophysicists. doi: 10.1190/1.3513325

Chiu, S. N., Stoyan, D., Kendall, W. S., & Mecke, J. (2013). *Stochastic geometry and its applications* (3rd ed.). John Wiley & Sons, Ltd. doi: 10.1002/9781118658222

Darcel, C., Bour, O., & Davy, P. (2003a). Cross-correlation between length and position in real fracture networks. *Geophysical Research Letters*, *30*(12). doi: 10.1029/2003GL017174

Darcel, C., Bour, O., & Davy, P. (2003b). Stereological analysis of fractal fracture networks. *Journal of Geophysical Research: Solid Earth*, *108*(B9). doi: 10.1029/2002JB002091

Davy, P., Le Goc, R., Darcel, C., Bour, O., de Dreuzy, J. R., & Munier, R. (2010). A likely universal model of fracture scaling and its consequence for crustal hydromechanics. *Journal of Geophysical Research*, *115*(B10). Retrieved 2015-07-01, from `http://doi.wiley.com/10.1029/2009JB007043` doi: 10.1029/2009JB007043

Dershowitz, W., & Einstein, H. H. (1988). Characterizing rock joint geometry with joint system models. *Rock Mechanics and Rock Engineering*, *21*(1), 21–51. doi: 10.1007/BF01019674

Dershowitz, W., & Herda, H. H. (1992). Interpretation of fracture spacing and intensity. In *The 33th US Symposium on Rock Mechanics (USRMS).* American Rock Mechanics Association.

Dershowitz, W., Mauldon, M., & La Pointe, P. (2020). Fracture abundance measures. In *54th US Rock Mechanics/Geomechanics Symposium.*

Gillespie, P. A., Howard, C. B., Walsh, J. J., & Watterson, J. (1993). Measurement and characterisation of spatial distributions of fractures. *Tectonophysics*, *226*(1), 113–141. doi: 10.1016/0040-1951(93)90114-Y

Gillespie, P. A., Johnston, J. D., Loriga, M. A., McCaffrey, K. J. W., Walsh, J. J., & Watterson, J. (1999). Influence of layering on vein systematics in line samples. *Geological Society, London, Special Publications*, *155*(1), 35–56. doi: 10.1144/GSL.SP.1999.155.01.05

Gomez-Rivas, E., Bons, P. D., Koehn, D., Urai, J. L., Arndt, M., Virgo, S., ... Blum, P. (2014). The Jabal Akhdar dome in the Oman Mountains: Evolution of a dynamic fracture system. *American Journal of Science*, *314*(7), 1104–1139. doi: 10.2475/07.2014.02

Hardebol, N. J., Maier, C., Nick, H., Geiger, S., Bertotti, G., & Boro, H. (2015). Multiscale fracture network characterization and impact on flow: A case study on the Latemar carbonate platform. *Journal of Geophysical Research: Solid Earth*, *120*(12), 8197–8222. doi: 10.1002/2015JB011879

Hentschel, H., & Procaccia, I. (1983). The infinite number of generalized dimensions of fractals and strange attractors. *Physica D: Nonlinear Phenomena*, *8*(3), 435–444. doi: 10.1016/0167-2789(83)90235-X

Hilgers, C., Kirschner, D. L., Breton, J.-P., & Urai, J. L. (2006). Fracture sealing and fluid overpressures in limestones of the Jabal Akhdar dome, Oman Mountains. *Geofluids*, *6*(2), 168–184. doi: 10.1111/j.1468-8123.2006.00141.x

Holland, M., Saxena, N., & Urai, J. L. (2009). Evolution of fractures in a highly dynamic thermal, hydraulic, and mechanical system - (II) Remote sensing fracture analysis, Jabal Shams, Oman Mountains. *GeoArabia*, *14*(3), 163–194. (Publisher: Gulf PetroLink)

Holland, M., Urai, J. L., Muchez, P., & Willemse, E. J. (2009). Evolution of fractures in a highly dynamic thermal, hydraulic, and mechanical system - (I) Field observations in Mesozoic Carbonates, Jabal Shams, Oman Mountains. *GeoArabia*, *14*(1), 57–110. (Publisher: Gulf PetroLink)

Illian, J., Penttinen, A., Stoyan, H., & Stoyan, D. (2008). *Statistical analysis and*

modelling of spatial point patterns. Chichester, UK: John Wiley & Sons, Ltd. doi: 10.1002/9780470725160

Ivanova, V. M., Sousa, R., Murrihy, B., & Einstein, H. H. (2014). Mathematical algorithm development and parametric studies with the GEOFRAC three-dimensional stochastic model of natural rock fracture systems. *Computers & Geosciences*, *67*, 100–109. doi: 10.1016/j.cageo.2013.12.004

Josnin, J.-Y., Jourde, H., Fénart, P., & Bidaux, P. (2002). A three-dimensional model to simulate joint networks in layered rocks. *Canadian Journal of Earth Sciences*, *39*(10), 1443–1455. Retrieved 2015-06-30, from `http://www.nrcresearchpress.com/doi/abs/10.1139/e02-043` doi: 10.1139/e02-043

Koike, K., Kubo, T., Liu, C., Masoud, A., Amano, K., Kurihara, A., ... Lanyon, B. (2015). 3D geostatistical modeling of fracture system in a granitic massif to characterize hydraulic properties and fracture distribution. *Tectonophysics*, *660*, 1–16. doi: 10.1016/j.tecto.2015.06.008

Lantuéjoul, C. (1978). Computation of the histograms of the number of edges and neighbours of cells in a tessellation. In R. Miles & J. Serra (Eds.), *Geometrical Probability and Biological Structures: Buffon's 200th Anniversary* (Vol. 23, pp. 323–329). Berlin: Springer.

Laubach, S. E., Lander, R. H., Criscenti, L. J., Anovitz, L. M., Urai, J. L., Pollyea, R. M., ... Pyrak-Nolte, L. (2019). The role of chemistry in fracture pattern development and opportunities to advance interpretations of geological materials. *Reviews of Geophysics*, *57*(3), 1065–1111. Retrieved 2022-01-21, from `https://onlinelibrary.wiley.com/doi/10.1029/2019RG000671` doi: 10.1029/2019RG000671

Lei, Q., Latham, J.-P., & Tsang, C.-F. (2017). The use of discrete fracture networks for modelling coupled geomechanical and hydrological behaviour of fractured rocks. *Computers and Geotechnics*, *85*, 151–176. doi: 10.1016/j.compgeo.2016.12.024

Macé, L., Souche, L., & Mallet, J.-L. (2004). 3D Fracture characterization based on geomechanics and geologic data uncertainties. In *ECMOR IX - 9th European Conference on the Mathematics of Oil Recovery*. Cannes, France: European Association of Geoscientists & Engineers. doi: 10.3997/2214-4609-pdb.9.A025

Manzocchi, T. (2002). The connectivity of two-dimensional networks of spatially correlated fractures. *Water Resources Research*, *38*(9), 1–1–1–20. doi: 10.1029/2000WR000180

Miles, R. (1974). On the elimination of edge effects in planar sampling. In R. Davidson, D. G. Kendall, & E. F. Harding (Eds.), *Stochastic geometry: a tribute to the memory of Rollo Davidson* (Vol. 10, pp. 228–247). London, New York: Wiley.

Odling, N. E. (1997). Scaling and connectivity of joint systems in sandstones from western Norway. *Journal of Structural Geology*, *19*(10), 1257–1271. doi: 10.1016/S0191-8141(97)00041-2

Odling, N. E., Gillespie, P., Bourgine, B., Castaing, C., Chiles, J. P., Christensen, N. P., ... Watterson, J. (1999). Variations in fracture system geometry and their implications for fluid flow in fractures hydrocarbon reservoirs. *Petroleum Geoscience*, *5*(4), 373–384. doi: 10.1144/petgeo.5.4.373

Peacock, D., & Sanderson, D. (2018). Structural analyses and fracture network characterisation: Seven pillars of wisdom. *Earth-Science Reviews*, *184*, 13–28. doi: 10.1016/j.earscirev.2018.06.006

Pyrcz, M., & Deutsch, C. V. (2014). *Geostatistical reservoir modeling* (Second edition ed.). Oxford: New York, New York : Oxford University Press.

Renard, P., & Allard, D. (2013). Connectivity metrics for subsurface flow and transport. *Advances in Water Resources*, *51*, 168–196. doi: 10.1016/j.advwatres

.2011.12.001

Saevik, P. N., & Nixon, C. W. (2017). Inclusion of topological measurements into analytic estimates of effective permeability in fractured media: fracture permeability from topology. *Water Resources Research*, *53*(11), 9424–9443. doi: 10.1002/2017WR020943

Sanderson, D. J., & Nixon, C. W. (2015). The use of topology in fracture network characterization. *Journal of Structural Geology*, *72*, 55–66. doi: 10.1016/j.jsg.2015.01.005

Sanderson, D. J., & Nixon, C. W. (2018). Topology, connectivity and percolation in fracture networks. *Journal of Structural Geology*, *115*, 167–177. doi: 10.1016/j.jsg.2018.07.011

Sanderson, D. J., & Peacock, D. C. (2019). Line sampling of fracture swarms and corridors. *Journal of Structural Geology*, *122*, 27–37. doi: 10.1016/j.jsg.2019.02.006

Sanderson, D. J., Peacock, D. C., Nixon, C. W., & Rotevatn, A. (2019). Graph theory and the analysis of fracture networks. *Journal of Structural Geology*, *125*, 155–165. doi: 10.1016/j.jsg.2018.04.011

Shakiba, M., Lake, L. W., Gale, J. F., & Pyrcz, M. J. (2022). Multiscale spatial analysis of fracture arrangement and pattern reconstruction using Ripley's K-function. *Journal of Structural Geology*, *155*, 104531. Retrieved 2022-02-02, from `https://linkinghub.elsevier.com/retrieve/pii/S0191814122000232` doi: 10.1016/j.jsg.2022.104531

Stoyan, D. (1994). Caution with "fractal" point patterns! *Statistics*, *25*(3), 267–270. doi: 10.1080/02331889408802450

Stoyan, D. (2021). Stochastic geometry in the geosciences. In B. Daya Sagar, Q. Cheng, J. McKinley, & F. Agterberg (Eds.), *Encyclopedia of Mathematical Geosciences* (pp. 1–10). Springer International Publishing.

Stoyan, D., & Stoyan, H. (1994). *Fractals, random shapes, and point fields: methods of geometrical statistics*. Chichester ; New York: Wiley.

Sui, L., Yu, J., Cang, D., Miao, W., Wang, H., Zhang, J., ... Chang, K. (2019). The fractal description model of rock fracture networks characterization. *Chaos, Solitons & Fractals*, *129*, 71–76. doi: 10.1016/j.chaos.2019.07.055

Wu, H., & D. Pollard, D. (1995). An experimental study of the relationship between joint spacing and layer thickness. *Journal of Structural Geology*, *17*(6), 887–905. Retrieved 2022-02-28, from `https://linkinghub.elsevier.com/retrieve/pii/019181419400099L` doi: 10.1016/0191-8141(94)00099-L

Zeeb, C., Gomez-Rivas, E., Bons, P. D., & Blum, P. (2013). Evaluation of sampling methods for fracture network characterization using outcrops. *AAPG Bulletin*, *97*(9), 1545–1566. doi: 10.1306/02131312042